Article:
Biswas, S., Mavlankar, N.A., Panuganti, V. et al. (2026) Modulation of biomolecular condensation of alpha-synuclein variants by eprodisate. Communications Chemistry, 9 (1). 227. ISSN: 2399-3669

https://doi.org/10.1038/s42004-026-02032-4

communications chemistry

A Nature Portfolio journal

Article

https://doi.org/10.1038/s42004-026-02032-4

Modulation of biomolecular condensation of alpha-synuclein variants by eprodisate

Soumojit Biswas[1], Nimisha A. Mavlankar[2], Venkataharsha Panuganti[1], Asish Pal[2] & Ipsita Roy[1]

Aggregation of α-synuclein (α-SYN) into amyloid structures is closely associated with Parkinson's disease (PD). Prevention of α-SYN aggregation has been validated as a key strategy to manage PD. α-SYN undergoes liquid-liquid phase separation (LLPS) via biomolecular condensation that facilitates nucleation and amyloid formation in liquid droplets. In this work, the effect of eprodisate (a glycosaminoglycan mimetic) on the formation of biomolecular condensates by α-SYN and its pathology-relevant variants has been investigated. Eprodisate affected the formation of α-SYN condensates, increased the fluidity inside droplets and inhibited α-SYN from turning into amyloid. It also attenuated aggregation of α-SYN variants in the presence of chondroitin sulphate. Eprodisate inhibited phase separation, hydrogel formation and amyloid aggregation of PD-related α-SYN A30P, α-SYN S129D and C-terminal truncated variants. It reduced oxidative stress, decreased α-SYN-positive aggregates and increased cell survival. These findings show that eprodisate may be explored further as an ameliorative therapy in PD.

Biomolecular phase separation arises from multivalent interactions among proteins and/or ribonucleic acids, leading to demixing of a homogeneous solution into distinct phases. Intrinsically disordered proteins (IDPs) and those with intrinsically disordered regions (IDRs) constitute a major class of phase-separating proteins[1,2]. A key feature enabling liquid–liquid phase separation (LLPS) is multivalency, whereby proteins engage in numerous weak, transient interactions with multiple partners. IDPs undergo LLPS due to their structural flexibility and ability to form simultaneous contacts, having multivalency[3,4]. Such interactions between disordered and folded domains are the primary drivers of phase separation. α-Synuclein (α-SYN) is a prime example of this class, and functions mainly as a regulator of synaptic neurotransmission. It interacts with synaptic vesicles and SNARE complex proteins, facilitating vesicular trafficking, docking and endocytosis within the presynaptic terminal[5]. Additionally, it is implicated in mitochondrial homeostasis, calcium regulation, protein phosphorylation, gene expression, fatty acid binding and tumorigenesis[6–8].

Aberrant phase transitions in proteins are increasingly linked to neurodegenerative diseases. Prolonged confinement in liquid droplets leads to "molecular aging," where droplets mature into solid aggregates with time[9,10]. In Parkinson's disease, α-SYN forms toxic oligomers and amyloid fibrils[11,12]. Initiation of LLPS in α-SYN is driven by low-complexity domains in the N-terminus and non-amyloid β core (NAC) domain[13]. The initial monomeric protein forms liquid droplets at high concentrations via weak intermolecular interactions, influencing nucleation-dependent oligomerisation[14,15] and fibrillation through liquid–solid transition[10,16].

The change in the primary sequence of α-SYN due to mutations or post-translational modifications (PTMs) regulates its LLPS. PTMs such as C-terminal truncation and phosphorylation have been linked with PD pathology[17–19]. Truncated α-synuclein is abundant in Lewy bodies and exhibits enhanced aggregation propensity[20,21]. Deletion of C-terminus enhances phase separation of α-SYN under low salt concentrations[19]. The phosphomimetic S129E variant, mimicking S129 phosphorylation, enhances LLPS and promotes liquid-to-solid transition into amyloid-like aggregates[13,22], whereas the S129D variant accelerates dopaminergic neuron loss and motor deficits in PD models[23].

PD-associated mutations in α-SYN like A30P, H50Q, A53T, and A53E show minimal effects on LLPS compared to the wild type (WT) protein, whereas E46K mutant accelerates phase separation[24]. Enhanced LLPS and solidification have been seen with E46K and A53T mutants[13]. Mutations lowering saturation concentration may promote condensation and irreversible aggregation over time, though correlation with oligomer and fibril formation remains unclear[13,25,26]. As PTMs and mutations of α-SYN are associated with disease pathology, identifying modulators of LLPS and aggregation is of therapeutic interest[27,28].

Glycosaminoglycans (GAGs) are associated with α-SYN amyloid deposition, with heparan sulphate proteoglycans (HSPGs) detected in Lewy bodies[29], though this remains disputed[30]. Several GAGs accelerate α-SYN fibrillation[31,32], whereas heparin inhibits HS–α-SYN interaction and HSPG-mediated cellular uptake, thereby reducing fibril toxicity[33–35]. Eprodisate (1,3-propanedisulphonate) is a negatively charged, sulphonated molecule

[1]Department of Biotechnology, National Institute of Pharmaceutical Education and Research, S.A.S. Nagar, Mohali, India. [2]Chemical Biology Unit, Institute of Nano Science and Technology, Knowledge City, Mohali, India. e-mail: ipsita@niper.ac.in

having structural similarities to heparin sulphate[36]. This glycosaminoglycan mimetic displaces stabilizing glycosaminoglycans from amyloid scaffolds, thereby inhibiting amyloid deposition[37–39]. Clinical studies have shown benefits in amyloid A (AA) amyloidosis with renal involvement[40], although a Phase 3 trial (NCT01215747) did not meet its primary endpoint. Its effect on α-SYN phase separation or aggregation remains unexplored. As the clinical safety and tolerability of eprodisate have been established, in this work, we first investigated whether this molecule is able to modulate the formation of biomolecular condensates by α-SYN and its pathology-relevant variants. Next, the mechanism of eprodisate on LLPS of α-SYN variants was probed using rheological and fluorescence assays. Eprodisate reduced gel rigidity, most notably for C-terminal truncated α-SYN, the predominant form in Lewy bodies and improved cell survival in a synucleinopathy model.

Results and discussion

Sporadic and familial PD involve aggregation of WT α-SYN and its variants. Inhibition of aggregation of α-SYN is a validated strategy to regulate disease progression. However, no pharmacological inhibitor has entered clinical trials. Since eprodisate has a proven safety profile, the effect of the molecule on phase separation and aggregation kinetics of PD-relevant α-SYN variants was investigated.

Expression and purification of α-SYN variants

Upon amplification of *α-SYN A30P* from pRSETB-*α-SYN*, bands were observed at the expected position for pRSETB-*α-SYN A30P* (~3.3 kb) (Supplementary Fig. 1A). Hence, an annealing temperature of 60.3 °C was used for large-scale amplification and purification of plasmid. The purified product was digested with *Dpn*I at 37 °C for 1 h and used to transform competent cells of *Escherichia coli* DH5α followed by isolation of positive clones (Supplementary Fig. 1B). Restriction digestion of the recombinant plasmid (from clones) using *Nde*I and *Nhe*I yielded a drop-out band at ~420 bp of *α-SYN A30P* and confirmed the integrity of the plasmids (Supplementary Fig. 1C). Mutation was confirmed by sequencing (Supplementary Fig. 1D). For amplification of *α-SYN S129D*, the band was observed at the expected position for pRSETB-*α-SYN S129D* (~3.3 kb) (Supplementary Fig. 2A). The purified product was digested with *Dpn*I at 37 °C for 1 h and used to transform competent cells of *E. coli* DH5α and positive clones were isolated (Supplementary Fig. 2B). Restriction digestion of the recombinant plasmid using *Nde*I and *Nhe*I yielded a drop-out band at ~420 bp of *α-SYN S129D* and confirmed the integrity of the plasmid (Supplementary Fig. 2C). Mutation was confirmed by sequencing (Supplementary Fig. 2D).

For amplification of *α-SYN CT*, bands were observed at all annealing temperatures at the expected position for *CT α-SYN* (~360 bp) (Supplementary Fig. 3A). The purified pRSETB vector backbone yielded a band at ~2.9 kb (Supplementary Fig. 3B). After ligation and transformation, positive clones were picked and plasmid isolation was performed. After restriction digestion, the expected dropout of *α-SYN CT* was seen at ~360 bp (Supplementary Fig. 3C, lanes 3 and 4). Amplification by PCR also showed bands at ~360 bp (Supplementary Fig. 3C, lanes 5 and 6).

Recombinant human WT α-SYN and its variants were expressed and purified by anion-exchange chromatography[11,41]. A single band in the eluate at the expected position confirmed the purification of WT α-SYN (Fig. 1A). The protein was confirmed by immunoblotting (Fig. 1B). Similarly, purification of α-SYN A30P (Fig. 1C, D), α-SYN S129D (Fig. 1E, F) and CT α-SYN (Fig. 1G, H) was confirmed.

Liquid–liquid phase separation of α-SYN variants

In the presence of a molecular crowder, viz. 10% PEG8000, soluble WT α-SYN (Supplementary Fig. 4A) formed highly dynamic spherical liquid-like droplets after 48 h (day 2, d2) (Fig. 2A and Supplementary Fig. 4B). This is similar to what has been reported for the wild-type protein earlier[13,16,42,43]. This could be due to reduced diffusion rates of droplets amidst high viscosity in the presence of the crowding agent resulting in delayed nucleation. Transmission electron micrographs of droplets formed at d5, d10, and d20 were also recorded (Supplementary Fig. 4C–E, respectively). Thus, PEG-induced macromolecular crowding increases the local effective protein

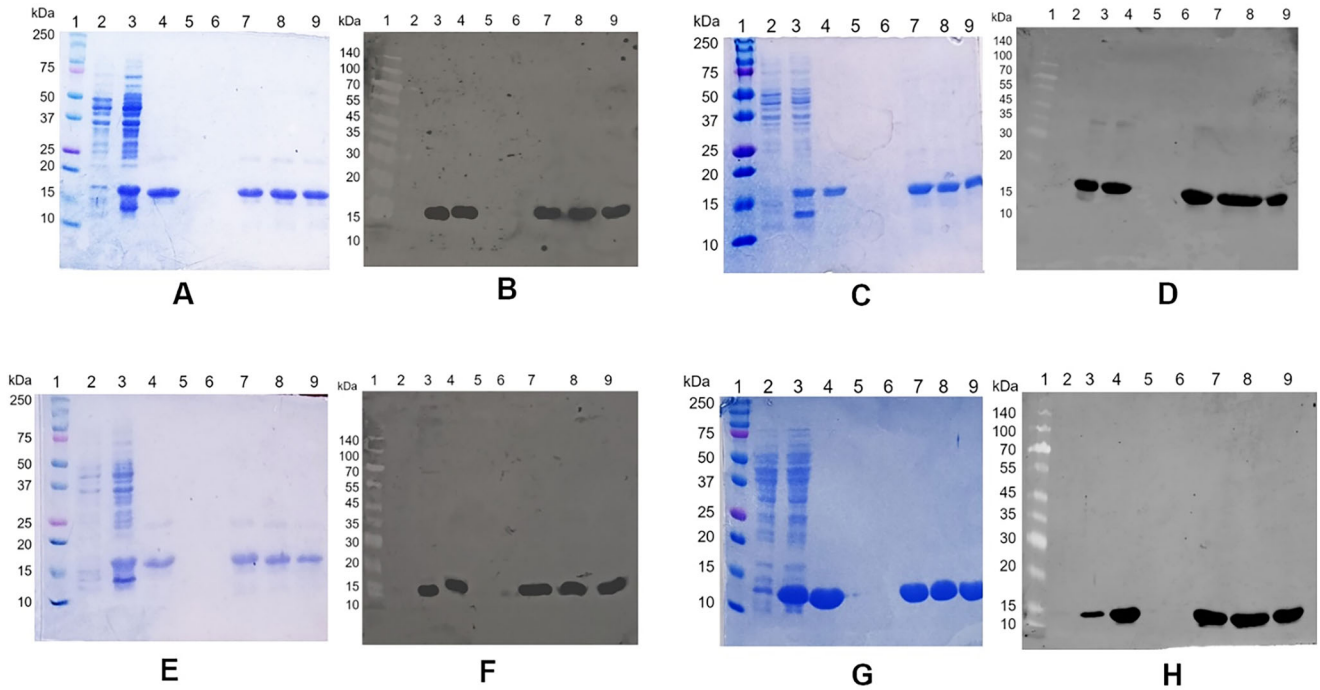

Fig. 1 | Expression and purification of α-SYN variants. A, **B** wild type α-SYN (WT α-SYN), (**C**, **D**) α-SYN A30P, (**E**, **F**) α-SYN S129D and (**G**, **H**) C-terminal truncated α-SYN (CT α-SYN). Purification was followed by (**A**, **C**, **E**, **G**) SDS PAGE and confirmed by western blotting using (**B**, **D**, **F**) rabbit monoclonal anti-α-SYN antibody or (**H**) rabbit polyclonal α-SYN (1-10 amino acid) antibody. Lane 1: Molecular weight markers, Lane 2: Lysate (uninduced), Lane 3: Lysate 1 (induced), Lane 4: Lysate 2 (induced), Lane 5: Flowthrough, Lane 6: Wash, Lane 7: Eluate 1, Lane 8: Eluate 2, Lane 9: Dialyzed protein.

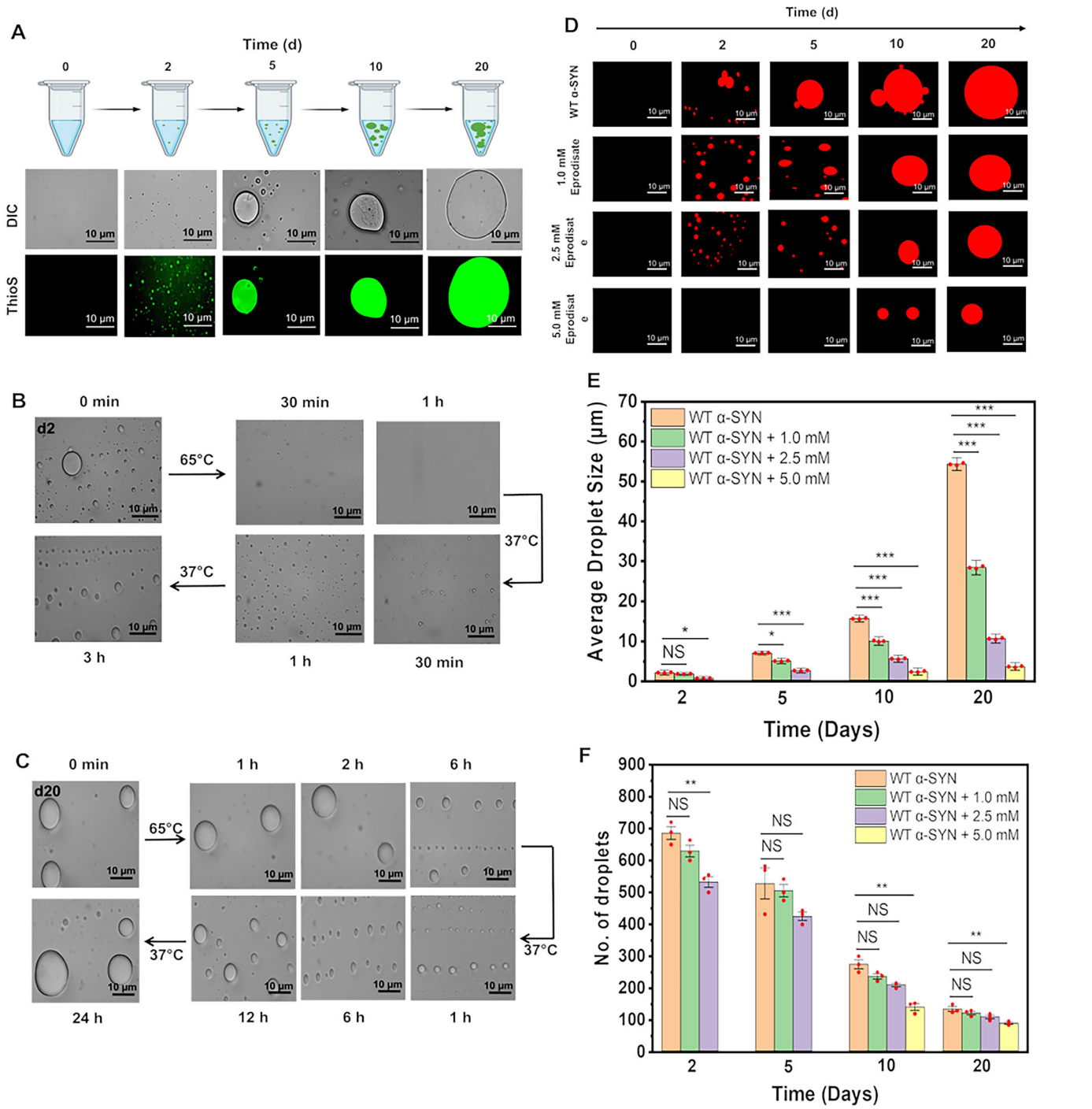

concentration and protein association, causing liquid–liquid phase separation (LLPS) of WT α-SYN. Thioflavin S (ThioS) is a small dye molecule that specifically binds to amyloids. ThioS staining of WT α-SYN was carried out. Non-specific staining was seen at the beginning of phase separation (d2) (Fig. 2A). At later time points (d5 onwards), ThioS was seen to stain the interior of the droplets, suggesting the formation of amyloid-like fibrils during the maturation of droplets. Higher intensity of ThioS was seen at d5, d10 and d20, suggesting fibril formation (Supplementary Fig. 5).

Phase-separated WT α-SYN condensates display characteristic features such as temperature reversibility and droplet fusion[44]. Early-stage droplets (d2) formed with 10% PEG8000 disappeared upon heating at 65 °C and reappeared on cooling to 37 °C, confirming their liquid-like and reversible nature (Fig. 2B). In contrast, aged droplets (d20) showed reduced size after prolonged heating and slower recovery upon cooling, indicating retained but delayed reversibility (Fig. 2C). Droplets formed by α-SYN were microscopically examined at various time intervals during the entire LLPS process. The liquid-like property of the WT α-SYN condensates was supported by the fusion events at d2 (Fig. 2D, Supplementary Movie 1). Coalescence of two droplets to form larger-sized droplets was seen with time (d5 and d10 of incubation) at 37 °C (Fig. 2D, Supplementary Movie 2 and Supplementary Movie 3, respectively). In addition to fusion, the droplet size gradually increased at the expense of nearby smaller droplets suggesting the possible mechanism of Ostwald ripening for droplet growth[45].

The liquid droplets formed by WT α-SYN in the absence and presence of eprodisate at various time intervals were examined under a microscope (Fig. 2D). Eprodisate decreased the size as well as the number (Fig. 2E, F) of

Fig. 2 | Phase separation of wild type α-SYN (WT α-SYN) in vitro. A ThioS staining of phase-separated wild type α-SYN (WT α-SYN) droplets over time. ThioS (20 μM, in 20 mM Tris HCl pH 7.8) was mixed with LLPS reaction mixture (200 μM WT α-SYN protein and 10% PEG8000) and was incubated at 37 °C. WT α-SYN incubated with ThioS exhibits green fluorescence. Images were visualized under 100X objective and 10X eyepiece. Bar = 10 μm. Quantification of ThioS staining is shown in Supplementary Fig. 5. **B** Differential interference contrast (DIC) images showing temperature-dependent reversibility of WT α-SYN phase-separated droplets in the presence of 10% PEG8000 after 2 days of incubation. Bar = 10 μm. **C** DIC images showing temperature-dependent irreversibility of α-SYN phase-separated droplets in the presence of 10% PEG8000 after 20 days of incubation. Bar = 10 μm. **D** Representative fluorescence microscopy images showing the formation of rhodamine-labeled WT α-SYN phase-separated condensates in the absence or presence of eprodisate. Bar = 10 μm. Rhodamine-labeled WT α-SYN (200 μM) was incubated in the presence of 10% PEG8000 and with different concentrations of eprodisate at 37 °C. WT α-SYN labeled with Rhodamine B exhibits red fluorescence. Microscopy images were recorded at different time intervals, and the average droplet size and number of droplets were quantified by ImageJ software. The size and number of droplets were counted from ten different microscopic fields (100X magnification). Corresponding DIC images are shown in Supplementary Fig. 6A. **E** For size distribution, $^{***}p < 0.001$, $^{*}p < 0.05$, and NS, non-significant against WT α-SYN in the absence of eprodisate. *p*-values for WT α-SYN + 1.0 mM eprodisate at day 2 (NS = 0.0871), WT α-SYN + 2.5 mM eprodisate at day 2 ($^{*}p = 0.0421$), WT α-SYN + 1.0 mM eprodisate at day 5 ($^{*}p = 0.0325$), WT α-SYN + 2.5 mM eprodisate at day 5 ($^{***}p = 0.0001$), WT α-SYN + 1.0 mM eprodisate at day 10 ($^{***}p = 0.00004$), WT α-SYN + 2.5 mM eprodisate at day 10 ($^{***}p = 0.00003$), WT α-SYN + 5.0 mM eprodisate at day 10 ($^{***}p = 0.00002$), WT α-SYN + 1.0 mM eprodisate at day 20 ($^{***}p = 0.00005$), WT α-SYN + 2.5 mM eprodisate at day 20 ($^{***}p = 0.00008$), WT α-SYN + 5.0 mM eprodisate at day 20 ($^{***}p = 0.00007$) are calculated with respect to WT α-SYN in the absence of eprodisate. **F** For number distribution, $^{**}p < 0.01$ and NS, non-significant against WT α-SYN in the absence of eprodisate. *p*-values for WT α-SYN + 1.0 mM eprodisate at day 2 (NS = 0.1097), WT α-SYN + 2.5 mM eprodisate at day 2 ($^{**}p = 0.0042$), WT α-SYN + 1.0 mM eprodisate at day 5 (NS = 0.6860), WT α-SYN + 2.5 mM eprodisate at day 5 (NS = 0.1087), WT α-SYN + 1.0 mM eprodisate at day 10 (NS = 0.8359), WT α-SYN + 2.5 mM eprodisate at day 10 (NS = 0.1350), WT α-SYN + 5.0 mM eprodisate at day 10 ($^{**}p = 0.0169$), WT α-SYN + 1.0 mM eprodisate at day 20 (NS = 0.2591), WT α-SYN + 2.5 mM eprodisate at day 20 (NS = 0.0653), WT α-SYN + 5.0 mM eprodisate at day 20 ($^{**}p = 0.0061$) are calculated with respect to WT α-SYN in the absence of eprodisate. For **E** and **F**, orange bars represent WT α-SYN, green bars represent WT α-SYN in the presence of 1.0 mM eprodisate, purple bars represent WT α-SYN in the presence of 2.5 mM eprodisate and yellow bars represent WT α-SYN in the presence of 5.0 mM eprodisate. The significance of the data is analyzed with the help of one-way ANOVA followed by Tukey's multiple comparison test with a 95% confidence interval. All the experiments were performed three times with similar observations and red dots indicate individual experimental replicates. Source data are provided in Supplementary Data 1.

WT α-SYN condensates. The average droplet size of WT α-SYN condensate was ~ 2 μm at d2 (Fig. 2D, E). This was found to increase gradually to 7 μm, 16 μm and 54 μm after d5, d10, and d20, respectively. In the presence of eprodisate, the formation of α-SYN droplets was inhibited efficiently in a concentration-dependent manner (Fig. 2E). The rhodamine-labeled protein also showed a similar effect in the presence of eprodisate (Supplementary Fig. 6A). The number of α-SYN droplets was also found to decrease with time. In the presence of eprodisate, further decrease in the number of droplets was seen in a concentration-dependent manner (Fig. 2D, F). Upon phase separation, highly mobile spherical droplets undergo frequent fusion events to form large condensate indicating their fluid-like nature.

Similar trends were seen with all α-SYN variants studied. In the case of α-SYN A30P, droplets were seen to form with time (Fig. 3A, Supplementary Fig. 6B). The average size of the droplets increased with time (Fig. 3B) but was significantly lower than the droplets formed with WT α-SYN. No droplets were seen in the presence of 2.5 mM eprodisate at d2, indicating that eprodisate slowed down droplet formation of α-SYN A30P as compared to WT α-SYN. The number of droplets formed at d2 was also lower than WT α-SYN (Fig. 3C). Interestingly, despite initial differences at starting time points, both the size and the number of droplets were seen to be similar for WT α-SYN and α-SYN A30P in the presence of higher concentrations of eprodisate at d20. In case of the phosphomimetic α-SYN S129D variant too, the size of the droplets decreased significantly at 5 mM eprodisate (Fig. 3D, E, Supplementary Fig. 6C). The number of droplets was higher in case of WT α-SYN than α-SYN S129D at d2 (686 ± 20.2 v/s 872 ± 62.2) but the difference was only marginal in the presence of 5 mM eprodisate at d20 (90 ± 3.5 v/s 77 ± 4.6, respectively) (Fig. 3F). Droplets were formed very early in case of CT α-SYN (Fig. 3G, Supplementary Fig. 6D). The average droplet size of CT α-SYN was 10.8 ± 0.8 μm at d2 (Fig. 3H) as compared to 2.2 ± 0.2 μm for WT α-SYN (d2). No droplets were seen in the presence of 5 mM eprodisate in case of WT α-SYN till d5 (Fig. 2E), while droplets were seen to be formed even at d2 by CT α-SYN under this condition (Fig. 3H). The number of droplets formed by CT α-SYN was seen to increase with time (Fig. 3I) and was not significantly different from that of WT α-SYN (Fig. 2F). However, in the presence of 5 mM eprodisate, the number of droplets was higher in case of WT α-SYN than CT α-SYN at d20 (90 ± 3.5 v/s 67 ± 5.5).

Fluorescence polarization

Fluorescence polarization (FP) measures the rotation of a fluorescently tagged molecule in solution based on its mass and can be used to track the movement of the tagged molecule, such as when it assembles into larger structures. For example, aggregation of WT α-SYN slows down its rotation, resulting in higher FP values[46,47]. For WT α-SYN, a low FP value (~ 38 mP) was observed at d2 which indicated that α-SYN is primarily in its monomeric (single molecule) form (Fig. 4A). The FP value was seen to increase at ~ 90 mP (d5), ~ 135 mP (d10) and ~ 250 mP (d20) and reflected increasingly restricted rotation of the tagged protein. Taken together with increasing droplet size of WT α-SYN with time (Fig. 2D), increased FP can be taken as a measure of phase separation. In the presence of increasing concentration of eprodisate, FP was seen to decrease with time (Fig. 4A), suggesting a decrease in phase separation. Notably, the rate of diffusion of the droplets also slowed down with time (d2, d5 up to d10), hinting at the increased rigid nature of the droplets (Supplementary Movies 1–3). For α-SYN A30P, significantly lower polarization was observed even at d2 (Supplementary Fig. 7), suggesting lower rate of phase separation for this variant. This matched well with the smallest droplet size among all variants (Fig. 3B). Its FP continued to be low for the period of investigation, i.e., till d20. The presence of eprodisate suppressed phase separation further at all concentrations (Fig. 4B). No significant difference was seen in the polarization of the tagged WT α-SYN and the phosphomimetic variant α-SYN S129D over all time points (Supplementary Fig. 7). The phase separation was seen to be retarded in the presence of eprodisate at all concentrations (Fig. 4C). The polarization of tagged CT α-SYN was the highest among all variants and remained so upon incubation up to d20 (Supplementary Fig. 7). Still, the polarization was noticeably lower than the threshold limit of anisotropy of fluorescein, i.e., 470 mP[48]. Eprodisate was successful in reducing phase separation and fluorescence polarization in a concentration-dependent manner (Fig. 4D). Decreasing FP values with higher eprodisate concentrations indicate inhibition of α-synuclein LLPS by disrupting intermolecular interactions, preventing droplet fusion and promoting smaller, more dynamic species.

Rheology measurements

Rheology is a valuable tool to assess phase transitions and aggregation behavior in amyloid-like proteins. It measures material stiffness and viscoelasticity, reflecting network complexity and cell interactions[49–51] and effectively captures sol–gel transitions induced by aggregation inhibitors[52]. We started our investigation with dynamic oscillatory amplitude sweep experiments for WT α-SYN incubated for 20 days to determine the linear viscoelastic (LVE) region in a plot of moduli vs strain %. WT α-SYN showed 1 order higher storage modulus (G' = 7136 Pa) than its loss modulus (G'' = 734 Pa), ($G' > G''$) indicative of its gel-like elastic behavior (Supplementary

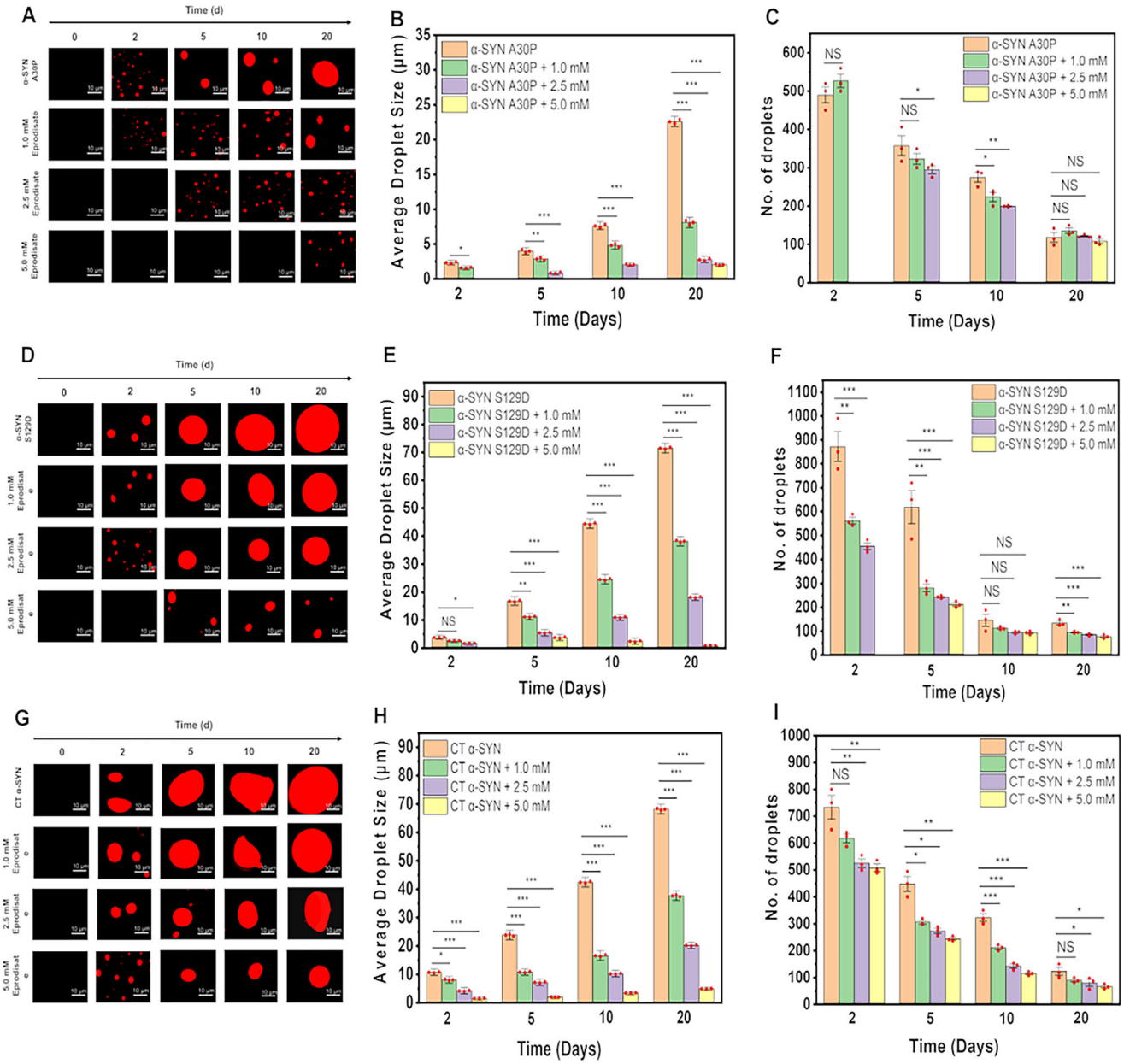

Fig. 8A)[53,54]. The frequency sweep bulk rheology measurement of WT α-SYN hydrogel at d20 showed a frequency independent behavior (Fig. 5A). Such hydrogel formation could be attributed to hydrophobic collapse and molecular crowding during the process of agglomeration[13]. We therefore monitored the aggregation process in the variants over time, particularly for 0, 5, and 20 days (Fig. 5B). A typical amplitude sweep study demonstrated higher yield stress values over time due to aggregation (Supplementary Figs. 8B-D). At the cross-over point of *G'*, *G"* the decline in *G'* indicated the hydrogel's stability dependence on applied strain. WT α-SYN transitioned to a viscous liquid with the least strain, followed by α-SYN A30P and α-SYN S129D, with CT α-SYN requiring the maximum strain for this shift. Time dependent evolution of storage moduli for variants as seen in Fig. 5B showed a gradual increase with highest mechanical strength achieved for CT α-SYN at all time points. Such behavior pointed towards higher aggregation propensity of CT α-SYN from the beginning of aggregation, whereas α-SYN A30P was found to sharp increase from 3.34 Pa at day 0 to 348 Pa at day 5 and 3212 Pa at day 20 indicative of dynamic phase transition. However, α-SYN S129D showed the slowest change in G′ over time. Tan δ, i.e., the damping factor/loss factor, is considered a better numerical descriptor of phase transition rather than the storage modulus. We therefore plotted tan δ as a function of time to estimate the liquid-like viscous behavior at the initial droplets' formation stage vs elastic-solid like gel after aggregation on ageing (Fig. 5C). When tan $\delta = 0$, the system is considered to be ideally elastic, while tan δ approaching infinity is interpreted as highly viscous behavior. Figure 5C clearly depicts the transition from viscous to elastic states for all four α-SYN variants with CT α-SYN showing the perfectly elastic behavior. Next, we examined the effect of eprodisate on aggregation inhibition. Addition of eprodisate reduced the gel strength of WT α-SYN significantly, by three orders of magnitude, in a concentration-dependent manner (Fig. 5D). In the presence of 5 mM eprodisate, the hydrogel exhibited lower storage (~800 Pa) and loss (~57 Pa) modulus as compared to the untreated control, indicating liquid-like behavior (Fig. 5A). The signals due to loss and storage moduli were seen to be noisy due to the weak character of the hydrogel formed by WT α-SYN in the presence of 5 mM eprodisate. Similar results were observed in amplitude sweep study of hydrogels treated with eprodisate (Supplementary Figs. 8A–D). These findings correlate with decreased fluorescence polarization in eprodisate-treated protein (Fig. 4A), indicating enhanced flexibility and a liquid-like state. A similar concentration-

Fig. 3 | Phase separation of α-SYN A30P, α-SYN S129D and C-terminal truncated α-SYN (CT α-SYN) in vitro. Proteins (200 μM) were labeled with rhodamine and incubated in the presence of 10% PEG8000 and with different concentrations of eprodisate at 37 °C. α-SYN variants labeled with Rhodamine B exhibits red fluorescence. At different time intervals, microscopy images were taken and the average droplet size and number of droplets were quantified by ImageJ software. The size and number of droplets were counted from ten different microscopic fields (100X magnification). **A** Representative fluorescence microscopy images showing the formation of rhodamine labeled α-SYN A30P phase separated condensates in the absence or presence of eprodisate. Bar = 10 μm. Corresponding DIC images are shown in Supplementary Fig. 6B. **B** For size distribution, $^{***}p < 0.001$, $^{*}p < 0.05$ and NS, non-significant against α-SYN A30P in the absence of eprodisate. *p*-values for α-SYN A30P + 1.0 mM eprodisate at day 2 ($^{*}p = 0.03125$), α-SYN A30P + 1.0 mM eprodisate at day 5 ($^{**}p = 0.0012$), α-SYN A30P + 2.5 mM eprodisate at day 5 ($^{***}p = 0.00003$), α-SYN A30P + 1.0 mM eprodisate at day 10 ($^{***}p = 0.00004$), α-SYN A30P + 2.5 mM eprodisate at day 10 ($^{***}p = 0.00007$), α-SYN A30P + 1.0 mM eprodisate at day 20 ($^{***}p = 0.00003$), α-SYN A30P + 2.5 mM eprodisate at day 20 ($^{***}p = 0.00002$), α-SYN A30P + 5.0 mM eprodisate at day 20 ($^{***}p = 0.00001$) are calculated with respect to α-SYN A30P in the absence of eprodisate. **C** For number distribution, $^{**}p < 0.01$ and NS, non-significant against α-SYN A30P in the absence of eprodisate. *p*-values for α-SYN A30P + 1.0 mM eprodisate at day 2 (NS = 0.2501), α-SYN A30P + 1.0 mM eprodisate at day 5 (NS = 0.3129), α-SYN A30P + 2.5 mM eprodisate at day 5 ($^{*}p = 0.0506$), α-SYN A30P + 1.0 mM eprodisate at day 10 ($^{*}p = 0.0435$), α-SYN A30P + 2.5 mM eprodisate at day 10 ($^{**}p = 0.0039$), α-SYN A30P + 1.0 mM eprodisate at day 20 (NS = 0.2957), α-SYN A30P + 2.5 mM eprodisate at day 20 (NS = 0.7913), α-SYN A30P + 5.0 mM eprodisate at day 20 (NS = 0.5187) are calculated with respect to α-SYN A30P in the absence of eprodisate. For panel B and C, orange bars represent α-SYN A30P, green bars represent α-SYN A30P in the presence of 1.0 mM eprodisate, purple bars represent α-SYN A30P in the presence of 2.5 mM eprodisate and yellow bars represent α-SYN A30P in the presence of 5.0 mM eprodisate. **D** Representative fluorescence microscopic images showing the formation of rhodamine labeled phosphomimetic α-SYN S129D phase-separated condensates in the absence or presence of eprodisate. Bar = 10 μm. Corresponding DIC images are shown in Supplementary Fig. 6C. **E** For size distribution, $^{***}p < 0.001$, $^{**}p < 0.01$, $^{*}p < 0.05$ and NS, non-significant against α-SYN S129D in the absence of eprodisate. *p*-values for α-SYN S129D + 1.0 mM eprodisate at day 2 (NS = 0.0945), α-SYN S129D + 2.5 mM eprodisate at day 2 ($^{*}p = 0.0263$), α-SYN S129D + 1.0 mM eprodisate at day 5 ($^{**}p = 0.0054$), α-SYN S129D + 2.5 mM eprodisate at day 5 ($^{***}p = 0.0002$), α-SYN S129D + 5.0 mM eprodisate at day 5 ($^{***}p = 0.0001$), α-SYN S129D + 1.0 mM eprodisate at day 10 ($^{***}p = 0.0002$), α-SYN S129D + 2.5 mM eprodisate at day 10 ($^{***}p = 0.00006$), α-SYN S129D + 5.0 mM eprodisate at day 10 ($^{***}p = 0.00007$), α-SYN S129D + 1.0 mM eprodisate at day 20 ($^{***}p = 0.00003$), α-SYN S129D + 2.5 mM eprodisate at day 20 ($^{***}p = 0.00005$), α-SYN S129D + 5.0 mM eprodisate at day 20 ($^{***}p = 0.00001$) are calculated with respect to α-SYN S129D in the absence of eprodisate. **F** For number distribution, $^{***}p < 0.001$, $^{**}p < 0.01$ and NS, non-significant against α-SYN S129D in the absence of eprodisate. *p*-values for α-SYN S129D + 1.0 mM eprodisate at day 2 ($^{**}p = 0.0082$), α-SYN S129D + 2.5 mM eprodisate at day 2 ($^{***}p = 0.0002$), α-SYN S129D + 1.0 mM eprodisate at day 5 ($^{**}p = 0.0092$), α-SYN S129D + 2.5 mM eprodisate at day 5 ($^{***}p = 0.0005$), α-SYN S129D + 5.0 mM eprodisate at day 5 ($^{***}p = 0.0004$), α-SYN S129D + 1.0 mM eprodisate at day 10 (NS = 0.2651), α-SYN S129D + 2.5 mM eprodisate at day 10 (NS = 0.1205), α-SYN S129D + 5.0 mM eprodisate at day 10 (NS = 0.1128), α-SYN S129D + 1.0 mM eprodisate at day 20 ($^{**}p = 0.0084$), α-SYN S129D + 2.5 mM eprodisate at day 20 ($^{***}p = 0.0004$), α-SYN S129D + 5.0 mM eprodisate at day 20 ($^{***}p = 0.0003$) are calculated with respect to α-SYN S129D in the absence of eprodisate. For **E** and **F**, orange bars represent α-SYN S129D, green bars represent α-SYN S129D in the presence of 1.0 mM eprodisate, purple bars represent α-SYN S129D in the presence of 2.5 mM eprodisate and yellow bars represent α-SYN S129D in the presence of 5.0 mM eprodisate. **G** Representative fluorescence microscopic images showing the formation of rhodamine labeled CT α-SYN (C-terminal truncated α-synuclein) phase-separated condensates in the absence or presence of eprodisate. Bar = 10 μm. Corresponding DIC images are shown in Supplementary Fig. 6D. **H** For size distribution, $^{***}p < 0.001$ and $^{*}p < 0.05$ against CT α-SYN in the absence of eprodisate. *p*-values for CT α-SYN + 1.0 mM eprodisate at day 2 ($^{*}p = 0.0253$), CT α-SYN + 2.5 mM eprodisate at day 2 ($^{***}p = 0.00056$), CT α-SYN + 5.0 mM eprodisate at day 2 ($^{***}p = 0.0008$), CT α-SYN + 1.0 mM eprodisate at day 5 ($^{***}p = 0.00045$), CT α-SYN + 2.5 mM eprodisate at day 5 ($^{***}p = 0.00038$), CT α-SYN + 5.0 mM eprodisate at day 5 ($^{***}p = 0.00011$), CT α-SYN + 1.0 mM eprodisate at day 10 ($^{***}p = 0.00015$), CT α-SYN + 2.5 mM eprodisate at day 10 ($^{***}p = 0.00038$), CT α-SYN + 5.0 mM eprodisate at day 10 ($^{***}p = 0.00016$), CT α-SYN + 1.0 mM eprodisate at day 20 ($^{***}p = 0.00062$), CT α-SYN + 2.5 mM eprodisate at day 20 ($^{***}p = 0.00056$), CT α-SYN + 5.0 mM eprodisate at day 20 ($^{***}p = 0.00023$) are calculated with respect to CT α-SYN in the absence of eprodisate. **I** For number distribution, $^{***}p < 0.001$, $^{**}p < 0.01$, $^{*}p < 0.05$ and NS, non-significant against CT α-SYN in the absence of eprodisate. *p*-values for CT α-SYN + 1.0 mM eprodisate at day 2 (NS = 0.0690), CT α-SYN + 2.5 mM eprodisate at day 2 ($^{**}p = 0.0113$), CT α-SYN + 5.0 mM eprodisate at day 2 ($^{**}p = 0.0082$), CT α-SYN + 1.0 mM eprodisate at day 5 ($^{*}p = 0.0073$), CT α-SYN + 2.5 mM eprodisate at day 5 ($^{*}p = 0.0038$), CT α-SYN + 5.0 mM eprodisate at day 5 ($^{**}p = 0.0018$), CT α-SYN + 1.0 mM eprodisate at day 10 ($^{***}p = 0.0001$), CT α-SYN + 2.5 mM eprodisate at day 10 ($^{***}p = 0.0003$), CT α-SYN + 5.0 mM eprodisate at day 10 ($^{***}p = 0.0001$), CT α-SYN + 1.0 mM eprodisate at day 20 (NS = 0.0973), CT α-SYN + 2.5 mM eprodisate at day 20 ($^{*}p = 0.0588$), CT α-SYN + 5.0 mM eprodisate at day 20 ($^{*}p = 0.0218$) are calculated with respect to CT α-SYN in the absence of eprodisate. For **H** and **I**, orange bars represent CT α-SYN, green bars represent CT α-SYN in the presence of 1.0 mM eprodisate, purple bars represent CT α-SYN in the presence of 2.5 mM eprodisate and yellow bars represent CT α-SYN in the presence of 5.0 mM eprodisate. The significance of the data is analyzed with the help of one-way ANOVA followed by Tukey's multiple comparison test with a 95% confidence interval. All the experiments were performed three times with similar observations. Red dots indicate individual experimental replicates. Source data are provided in Supplementary Data 1.

dependent decrease in storage modulus was observed for other variants, supporting effective aggregation inhibition (Fig. 5E; Supplementary Figs. 8E–G). To assess the stage of inhibition, eprodisate was added from day 0 and loss factor was monitored over time (Fig. 5F). Eprodisate-treated samples consistently showed lower tan δ, indicating reduced viscosity. Even at day 20, variants remained predominantly viscous and CT α-SYN failed to reach a fully elastic state, confirming effective aggregation inhibition by eprodisate.

Aggregation of α-SYN variants

Thioflavin T, a cationic benzothiazole dye, binds to cross β-sheet rich structures in fibrils, which leads to enhanced fluorescence of the dye[55]. The increase in fluorescence intensity of Th T confirmed the formation of cross-β-sheet rich structures by WT α-SYN upon incubation at different time intervals at 37 °C (Fig. 6A). As expected[11,12], aggregation kinetics of WT α-SYN followed a sigmoidal pattern with lag phase, log phase and stationary phase (Fig. 6A). Lag time of nucleation and apparent rate of fibrillation (k_{app}) of WT α-SYN in the presence of PEG were 28 h and 0.190 h^{-1}, respectively. The fibrillar nature of aggregates was confirmed by TEM (Supplementary Figs. 4F, 4G). Taken together with higher fluorescence polarization with time and rheological measurements, Th T studies show that WT α-SYN forms condensates, which are converted to fibrillar filaments with time. In the presence of eprodisate, reduction in aggregation of WT α-SYN in the presence of PEG was observed in a concentration-dependent manner, with the highest reduction being observed in the presence of 5 mM eprodisate (Fig. 6A). This was due to a delay in the formation of the threshold 'seed' with the lag time of nucleation increasing to 40 h and 52 h in the presence of 2.5 mM and 5 mM eprodisate, respectively. No significant difference was seen in the amount of fibrillar aggregates formed by any of the variants in the presence of eprodisate at the end point of measurement in the absence or presence of the crowding agent (Supplementary Fig. 9). Inhibition of amyloid formation was also confirmed by Thio S staining of the droplets (Supplementary Fig. 10A). The average size (Fig. 2E) and number (Fig. 2F) of droplets formed under these conditions were also reduced, providing a cause for the delayed formation of seeds. Along with this, k_{app} was seen to decrease with increasing concentration of eprodisate (0.100 h^{-1} and 0.070 h^{-1} in the presence of 2.5 mM and 5.0 mM eprodisate, respectively). Thus, oligomers are formed later and are

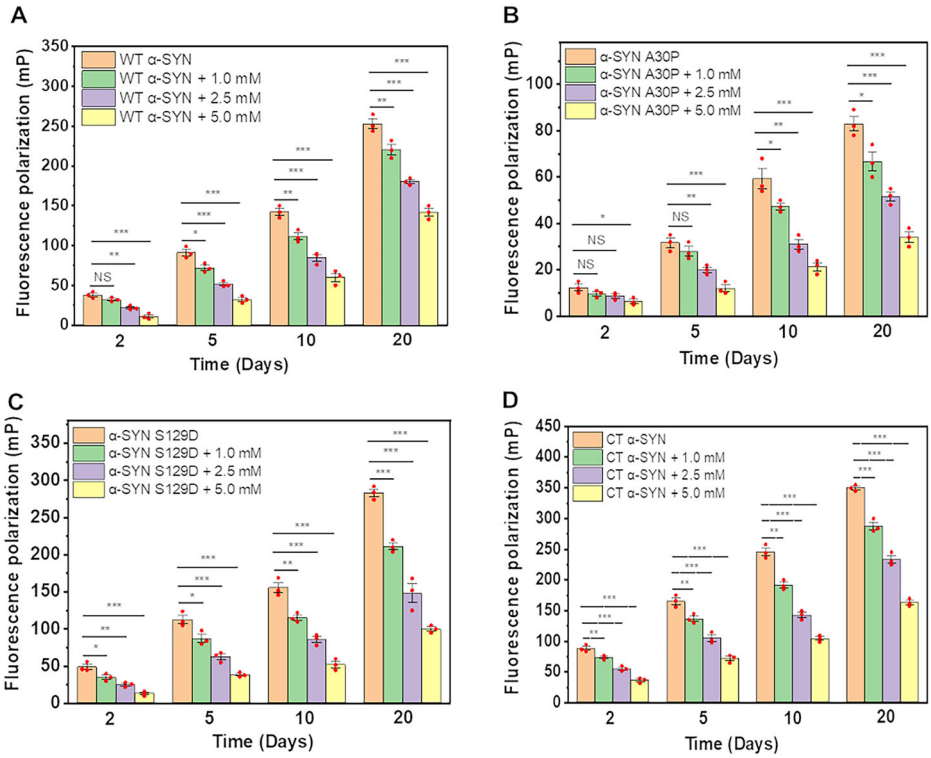

Fig. 4 | Fluorescence polarization analysis of labeled α-SYN variants. Changes in the rotational state of WT α-SYN^{488}, α-SYN A30P^{488}, α-SYN S129D^{488} and CT α-SYN^{488} were measured by FP as described in experimental procedures. Reactions were performed in 96-well plates, and individual samples were removed and measured at the indicated time points. Changes in FP relative to monomer (ΔmP) were measured, indicating that FP increases significantly following assembly. **A** Changes in the rotational state of WT α-SYN^{488} in the absence or presence of different concentrations of eprodisate. ***$p < 0.001$, **$p < 0.01$, *$p < 0.05$ and NS, non-significant against WT α-SYN in the absence of eprodisate. p-values for WT α-SYN + 1.0 mM eprodisate at day 2 (NS = 0.1063), WT α-SYN + 2.5 mM eprodisate at day 2 (**$p = 0.0044$), WT α-SYN + 5.0 mM eprodisate at day 2 (***$p = 0.0009$), WT α-SYN + 1.0 mM eprodisate at day 5 (*$p = 0.0205$), WT α-SYN + 2.5 mM eprodisate at day 5 (***$p = 0.0010$), WT α-SYN + 5.0 mM eprodisate at day 5 (***$p = 0.0002$), WT α-SYN + 1.0 mM eprodisate at day 10 (**$p = 0.0077$), WT α-SYN + 2.5 mM eprodisate at day 10 (***$p = 0.0007$), WT α-SYN + 5.0 mM eprodisate at day 10 (***$p = 0.0002$), WT α-SYN + 1.0 mM eprodisate at day 20 (**$p = 0.0022$), WT α-SYN + 2.5 mM eprodisate at day 20 (***$p = 0.0004$), WT α-SYN + 5.0 mM eprodisate at day 20 (***$p = 0.0001$) are calculated with respect to WT α-SYN in the absence of eprodisate. Orange bars represent WT α-SYN, green bars represent WT α-SYN in the presence of 1.0 mM eprodisate, purple bars represent WT α-SYN in the presence of 2.5 mM eprodisate and yellow bars represent WT α-SYN in the presence of 5.0 mM eprodisate. **B** Changes in the rotational state of α-SYN A30P^{488} in the absence or presence of different concentrations of eprodisate. ***$p < 0.001$, **$p < 0.01$, *$p < 0.05$ and NS, non-significant against α-SYN A30P in the absence of eprodisate. p-values for α-SYN A30P + 1.0 mM eprodisate at day 2 (NS = 0.1917), α-SYN A30P + 2.5 mM eprodisate at day 2 (NS = 0.0971), α-SYN A30P + 5.0 mM eprodisate at day 2 (*$p = 0.0242$), α-SYN A30P + 1.0 mM eprodisate at day 5 (NS = 0.2755), α-SYN A30P + 2.5 mM eprodisate at day 5 (**$p = 0.0074$), α-SYN A30P + 5.0 mM eprodisate at day 5 (***$p = 0.0014$), α-SYN A30P + 1.0 mM eprodisate at day 10 (*$p = 0.0597$), α-SYN A30P + 2.5 mM eprodisate at day 10 (**$p = 0.0042$), α-SYN A30P + 5.0 mM eprodisate at day 10 (***$p = 0.0012$), α-SYN A30P + 1.0 mM eprodisate at day 20 (*$p = 0.0343$), α-SYN A30P + 2.5 mM eprodisate at day 20 (***$p = 0.0011$), α-SYN A30P + 5.0 mM eprodisate at day 20 (***$p = 0.0002$) are calculated with respect to α-SYN A30P in the absence of eprodisate. Orange bars represent α-SYN A30P, green bars represent α-SYN A30P in the presence of 1.0 mM eprodisate, purple bars represent α-SYN A30P in the presence of 2.5 mM eprodisate and yellow bars represent α-SYN A30P in the presence of 5.0 mM eprodisate. **C** Changes in the rotational state of α-SYN S129D^{488} in the absence or presence of different concentrations of eprodisate. ***$p < 0.001$, **$p < 0.01$ and *$p < 0.05$ against α-SYN S129D in the absence of eprodisate. p-values for α-SYN S129D + 1.0 mM eprodisate at day 2 (*$p = 0.0369$), α-SYN S129D + 2.5 mM eprodisate at day 2 (**$p = 0.0038$), α-SYN S129D + 5.0 mM eprodisate at day 2 (***$p = 0.0008$), α-SYN S129D + 1.0 mM eprodisate at day 5 (*$p = 0.0311$), α-SYN S129D + 2.5 mM eprodisate at day 5 (***$p = 0.0018$), α-SYN S129D + 5.0 mM eprodisate at day 5 (***$p = 0.0002$), α-SYN S129D + 1.0 mM eprodisate at day 10 (**$p = 0.0064$), α-SYN S129D + 2.5 mM eprodisate at day 10 (***$p = 0.0009$), α-SYN S129D + 5.0 mM eprodisate at day 10 (***$p = 0.0003$), α-SYN S129D + 1.0 mM eprodisate at day 20 (***$p = 0.0005$), α-SYN S129D + 2.5 mM eprodisate at day 20 (***$p = 0.00006$), α-SYN S129D + 5.0 mM eprodisate at day 20 (***$p = 0.00002$) are calculated with respect to α-SYN S129D in the absence of eprodisate. Orange bars represent α-SYN S129D, green bars represent α-SYN S129D in the presence of 1.0 mM eprodisate, purple bars represent α-SYN S129D in the presence of 2.5 mM eprodisate and yellow bars represent α-SYN S129D in the presence of 5.0 mM eprodisate. **D** Changes in the rotational state of CT α-SYN^{488} in the absence or presence of different concentrations of eprodisate. ***$p < 0.001$ and **$p < 0.01$ against CT α-SYN in the absence of eprodisate. p-values for CT α-SYN + 1.0 mM eprodisate at day 2 (**$p = 0.0195$), CT α-SYN + 2.5 mM eprodisate at day 2 (***$p = 0.0012$), CT α-SYN + 5.0 mM eprodisate at day 2 (***$p = 0.0002$), CT α-SYN + 1.0 mM eprodisate at day 5 (**$p = 0.0146$), CT α-SYN + 2.5 mM eprodisate at day 5 (***$p = 0.0012$), CT α-SYN + 5.0 mM eprodisate at day 5 (***$p = 0.0001$), CT α-SYN + 1.0 mM eprodisate at day 10 (**$p = 0.0022$), CT α-SYN + 2.5 mM eprodisate at day 10 (***$p = 0.0001$), CT α-SYN + 5.0 mM eprodisate at day 10 (***$p = 0.00003$), CT α-SYN + 1.0 mM eprodisate at day 20 (***$p = 0.0007$), CT α-SYN + 2.5 mM eprodisate at day 20 (***$p = 0.00006$), CT α-SYN + 5.0 mM eprodisate at day 20 (***$p = 0.00002$) are calculated with respect to CT α-SYN in the absence of eprodisate. Orange bars represent CT α-SYN, green bars represent CT α-SYN in the presence of 1.0 mM eprodisate, purple bars represent CT α-SYN in the presence of 2.5 mM eprodisate and yellow bars represent CT α-SYN in the presence of 5.0 mM eprodisate. The significance of the data is analyzed by one-way Analysis of Variance (ANOVA) for multiple comparisons. Data represent mean ± sem for $n = 3$ independent experiments and red dots indicate individual experimental replicates. Source data are provided in Supplementary Data 1.

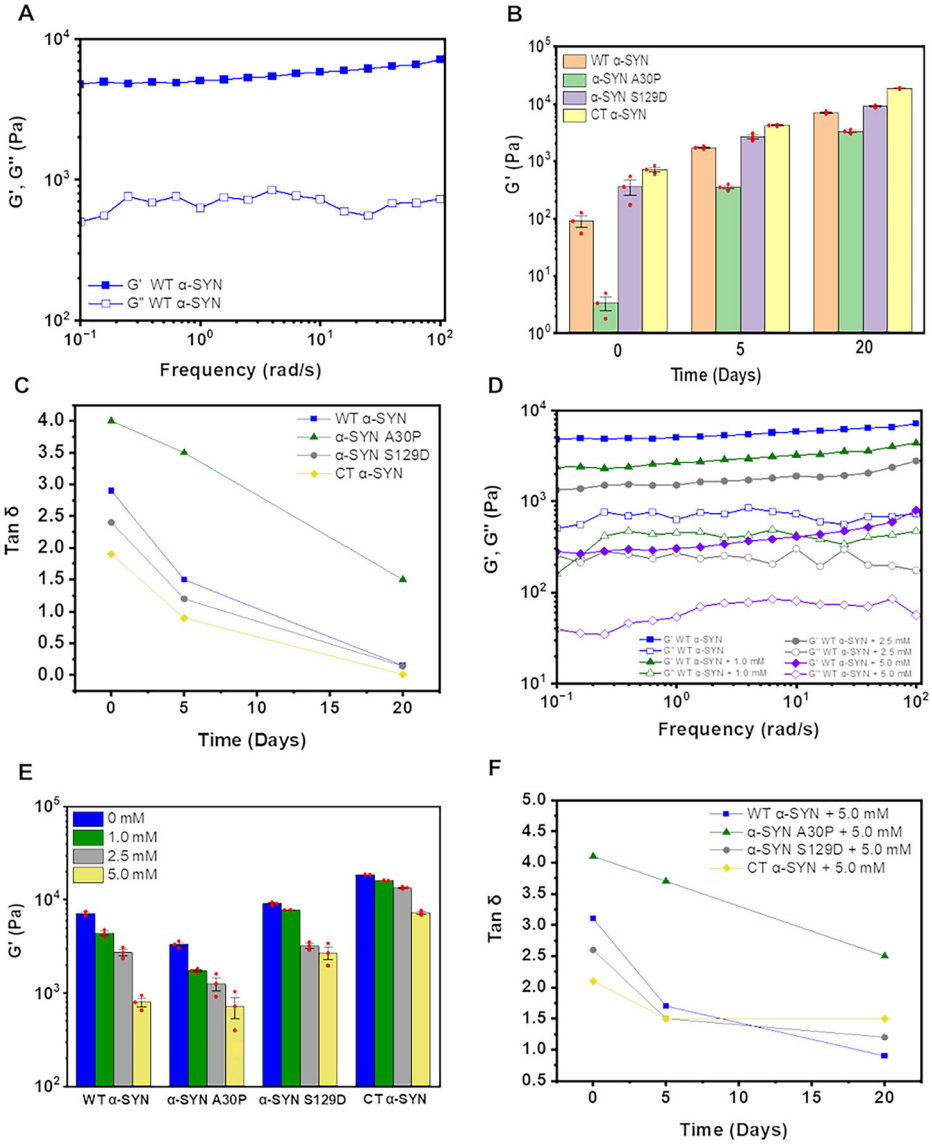

Fig. 5 | Rheological characterization of α-SYN and its variants in the absence or presence of different concentrations of eprodisate. A Frequency sweep of WT α-SYN gels showing G′ (blue filled square with solid line) and G″ (blue empty square with solid line) at a strain of 0.5% over a frequency range of 0.1–100 rad/s. **B** Histogram showing the comparison between the storage moduli, G′ of WT α-SYN and its variants over time. Orange bars represent WT α-SYN, green bars represent α-SYN A30P, purple bars represent α-SYN S129D and yellow bars represent C terminal truncated α-SYN (CT α-SYN) at day 0, day 5 and day 20, respectively. Red dots in bar graphs indicate individual experimental replicates. **C** Loss factor depicting phase transitions occurring in WT α-SYN and its variants over time. In **C**, WT α-SYN represent blue filled square with solid line, α-SYN A30P represent green filled triangle with solid line, α-SYN S129D represent gray filled circle with solid line and CT α-SYN represent yellow filled diamond with solid line. **D** Frequency sweep of WT α-SYN gels incubated with varying concentrations of eprodisate showing declining gel strength. For WT α-SYN, G′ is shown as blue filled square with solid lines and G″ is shown as blue empty square with solid lines. In the presence of eprodisate, 1.0, 2.5 and 5.0 mM are represented by green triangles, gray circles and purple diamonds, respectively, with G′ shown as filled symbols with solid lines and G″ as open symbols with solid lines. **E** Histogram showing the comparison between the storage moduli, G′ of α-SYN and its variants with 0 mM (blue bars), 1.0 mM (green bars), 2.5 mM (gray bars) and 5.0 mM (yellow bars) eprodisate, respectively. **F** Eprodisate mediated changes in loss factor for α-SYN and its variants as a function time. In **F**, WT α-SYN with 5 mM eprodisate represent blue filled square with solid line, α-SYN A30P with 5.0 mM eprodisate represent green filled triangle with solid line, α-SYN S129D with 5.0 mM eprodisate represent gray filled circle with solid line and CT α-SYN with 5.0 mM eprodisate represent yellow filled diamond with solid line. Data represent mean ± sem for n = 3 independent experiments. Source data are provided in Supplementary Data 1.

converted to mature aggregates faster. As oligomers are proposed to be the major toxic species formed during protein aggregation[56,57], lower residence time of oligomers in the presence of eprodisate is likely to be beneficial in disease conditions.

For α-SYN A30P, protein aggregation was significantly reduced as compared to WT α-SYN (Fig. 6B), with enhanced lag time (46 h) and k_{app} (0.200 h^{-1}) in the presence of PEG. The delay in fibrillation in the presence of eprodisate was confirmed by Thio S staining of the droplets (Supplementary Fig. 10B). This matched well with reduced phase separation (Fig. 4B) and lower storage and loss modulus (Fig. 5B) as compared with WT α-SYN. The lag time increased to 54 h and 58 h in the presence of 1 mM and 2.5 mM eprodisate, respectively. Lag time was not observed in the presence of 5 mM eprodisate (Fig. 6B).

In the case of phosphomimetic α-SYN S129D in the presence of PEG, the lag time of nucleation and k_{app} were found to be 20 h and 0.170 h^{-1}, respectively (Fig. 6C). The lag time increased to 31 h, 40 h and 44 h in the presence of 1.0 mM, 2.5 mM and 5.0 mM eprodisate, respectively (Fig. 6C). On the other hand, the apparent rate of fibrillation was seen to decrease with

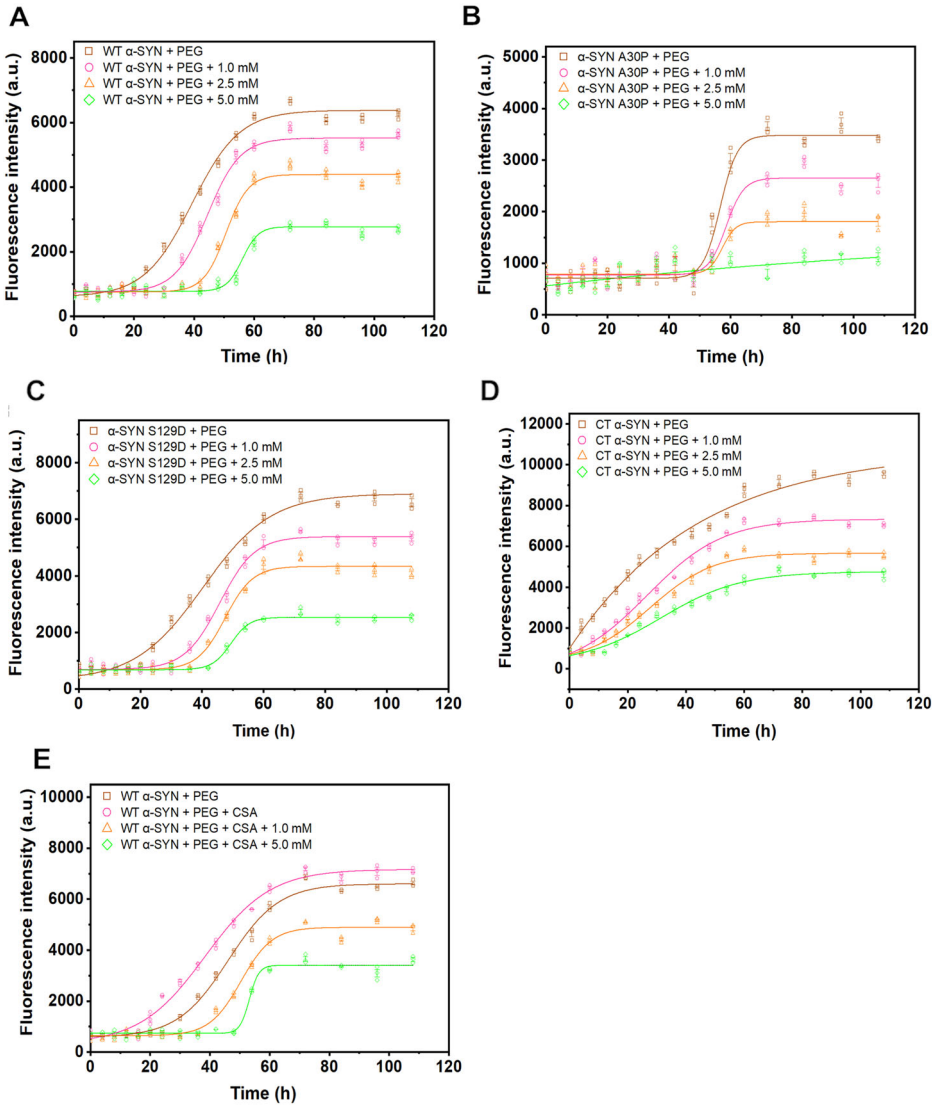

Fig. 6 | Aggregation kinetics of α-SYN and its variants in the absence or presence of different concentrations of eprodisate were monitored by Th T assay. A WT α-SYN; **B** α-SYN A30P; **C** α-SYN S129D; **D** C terminal truncated (CT) α-SYN; **E** WT α-SYN + 1 mM CSA + eprodisate. PEG was employed in these experiments. Final concentrations of 10 μM protein and 20 μM Th T were used for the assay (λ_{ex} 440 nm, λ_{em} 485 nm). For kinetic curves, WT α-SYN is shown as brown squares, 1.0 mM eprodisate as pink circles, 2.5 mM as orange triangles and 5.0 mM as green diamonds. The same color and symbol scheme was applied for α-SYN A30P, α-SYN S129D and CT α-SYN in **B**–**D**. For **E**, WT α-SYN with 1 mM CSA and increasing concentrations of eprodisate (1.0 and 5.0 mM), shown as pink circles, orange triangles and green diamonds, respectively; WT α-SYN alone is shown as brown squares. In **A**–**E**, solid lines represent Boltzmann fits to the data. Data represent mean ± sem for n = 3 independent experiments. Source data are provided in Supplementary Data 1.

increasing concentration of eprodisate. Thio S staining of the droplets confirmed eprodisate-induced delay in fibrillation (Supplementary Fig. 10C). Truncation of C-terminal end of α-SYN in the presence of PEG led to significant reduction in lag time (2 h) as compared to WT α-SYN, which increased to 6 h, 12 h and 18 h in the presence of 1.0 mM, 2.5 mM and 5.0 mM eprodisate, respectively (Fig. 6D). The apparent rate of fibrillation increased to 0.410 h^{-1}, as compared to WT α-SYN, and was seen to decrease to 0.290 h^{-1}, 0.100 h^{-1} and 0.070 h^{-1} in the presence of 1.0 mM, 2.5 mM and 5.0 mM eprodisate, respectively. Amyloid formation in the droplets was seen to be significantly delayed in the presence of eprodisate (Supplementary Fig. 10D). Thus, eprodisate reduced the strength of the hydrogel as well as the aggregation propensity of all variants of α-SYN.

Glycosaminoglycans (GAGs) and proteoglycans are present in amyloid deposits, including heparan sulphate proteoglycans in Lewy bodies[29]. Various GAGs such as heparin, heparan sulphate, *N*-acetyl heparan, chondroitin sulphate B, etc. can accelerate fibrillation of WT α-SYN in vitro[31]. Heparan sulphate facilitates intercellular propagation and uptake of α-SYN aggregates[58,59]. Treatment with heparin lyases and chondroitinase ABC disrupts GAG–aggregate interaction[59]. This interaction is less dependent on GAG structure than in tau aggregates[34] and GAG-deficient cells show reduced α-SYN uptake[59]. Since multiple lines of evidence suggest the important role that GAGs play in fibrillation of α-SYN and the ability of eprodisate to disrupt amyloid-GAG scaffold, the effect of eprodisate on GAG-mediated fibrillation of WT α-SYN was studied.

The amount of aggregates formed by WT α-SYN was higher in the presence of 1 mM CSA than in its absence (Fig. 6E). The lag time of nucleation was significantly reduced (17 h in the presence of 1 mM CSA as compared to 28 h in its absence) while k_{app} increased from 0.23 h^{-1} in the absence of CSA to 0.33 h^{-1} in its presence. The presence of eprodisate succeeded in reducing the amount of aggregates formed by WT α-SYN. The lag time was increased to 40 h and 50 h, and k_{app} was reduced to 0.20 h^{-1} and 0.10 h^{-1}, when WT α-SYN was incubated with 1 mM CSA in the presence of 1 mM and 5 mM eprodisate, respectively. The other variants, viz. α-SYN A30P (Supplementary Fig. 11A), α-SYN S129D (Supplementary Fig. 11B) and CT α-SYN (Supplementary Fig. 11C), were also incubated in the presence of 1 mM CSA. In case of α-SYN A30P, lag time was reduced by 15% while k_{app} was increased by 65%. A similar result was seen in case of α-SYN S129D, with lag time decreasing by 25% and k_{app} increasing by 100% in the presence of CSA. However, in case of CT α-SYN, no significant difference in lag time of nucleation of the protein was seen in the presence of CSA, likely because the protein alone exhibited significant fibrillation under the conditions of incubation (Fig. 6D). In the presence of 1 mM eprodisate, the lag time of nucleation of each protein was significantly longer in case of α-SYN A30P ((Supplementary Fig. 11A), α-SYN S129D (Supplementary Fig. 11B) and CT α-SYN (Supplementary Fig. 11C). A higher concentration of

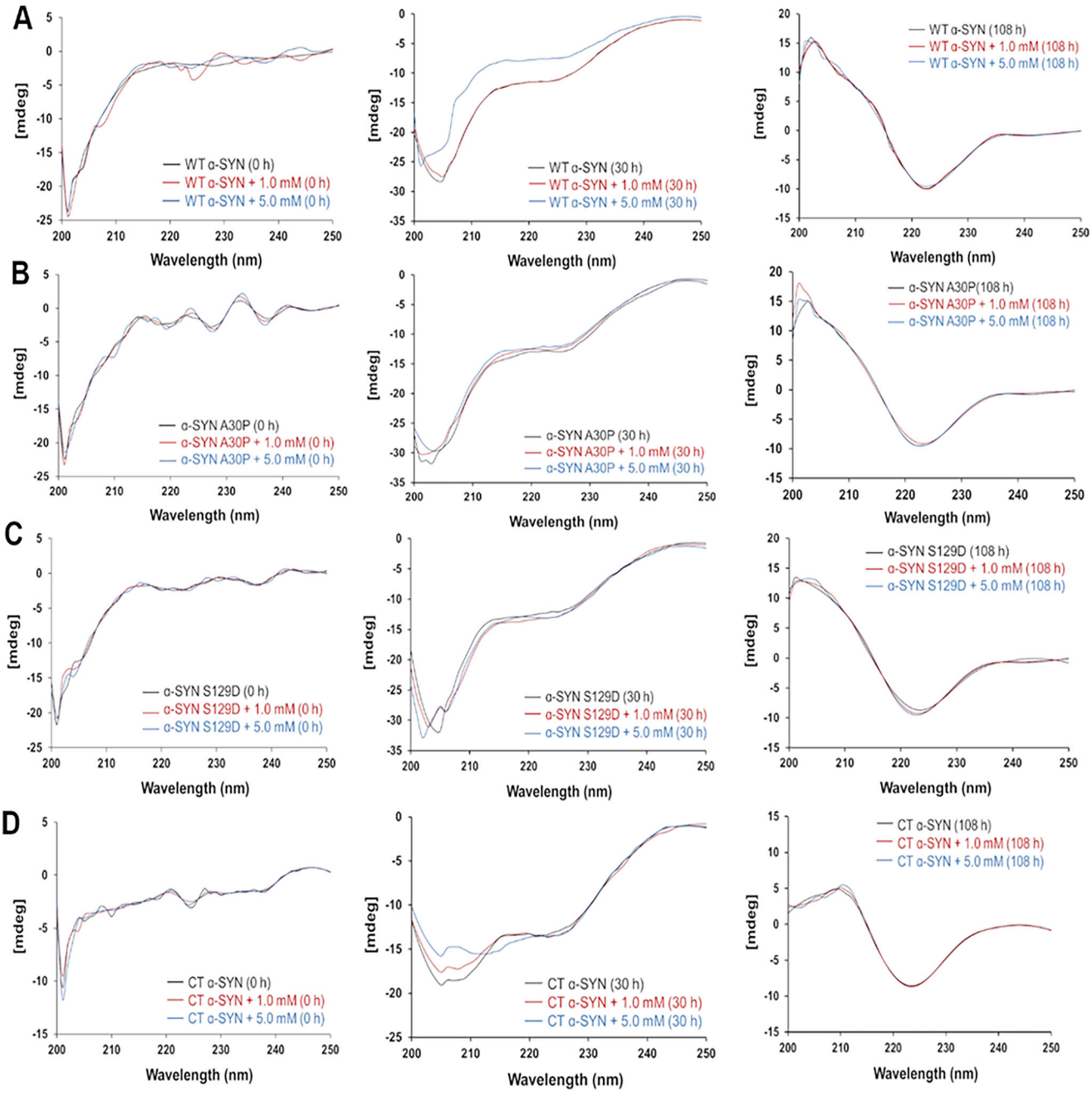

Fig. 7 | Effect of eprodisate on the secondary structure of α-SYN and its variants over time. Far UV CD spectra of **A** WT α-SYN, **B** α-SYN A30P, **C** α-SYN S129D and **D** C terminal truncated α-SYN (CT α-SYN) were recorded at different time points (0 h, 30 h and 108 h) in the absence and presence of 1 mM and 5 mM eprodisate. In all panels, black line represents protein alone, red line represents 1 mM eprodisate and blue line represents 5 mM eprodisate. Spectra are shown in millidegrees (mdeg) as a function of wavelength (200–250 nm). Source data are provided in Supplementary Data 1.

eprodisate (5 mM) was able to reduce the fibrillation of all three variants successfully even in the presence of CSA. In case of CT α-SYN, the aggregation-inhibitory effect of eprodisate was stronger in the presence of CSA (Supplementary Fig. 11C) than in its absence (Fig. 6D). Thus, eprodisate was successful in inhibiting aggregation of all variants of α-SYN in the presence of a competing GAG.

Changes in secondary structures of α-SYN variants

Changes in the secondary structure of α-SYN during phase separation were followed by far UV CD spectroscopy. WT α-SYN is a natively disordered protein and the same is seen in its CD spectrum with no distinct peak between 210-220 nm (Supplementary Fig. 12A, Fig. 7A)[11,60]. The same was observed for A30P α-SYN (Supplementary Fig. 12A, Fig. 7B) and S129D α-SYN (Supplementary Fig. 12A, Fig. 7C). The disorder was lower in case of CT α-SYN at 0 h (Supplementary Fig. 12A, Fig. 7D). Changes in structure were observed for all proteins at 30 h (formation of oligomers, Supplementary Fig. 12B) and 108 h (formation of mature fibrils, Supplementary Fig. 12C) and the spectrum of CT α-SYN was significantly different from that of other α-SYN variants at both these time points (Fig. 7). Incubation with eprodisate did not lead to any noticeable change in secondary structure of any of the variants at 0 h (Fig. 7A–D). For WT α-SYN, the most significant change in the spectrum occurred in the presence of 5 mM eprodisate during the formation of oligomers (30 h) (Fig. 7A). Further incubation caused no eprodisate-

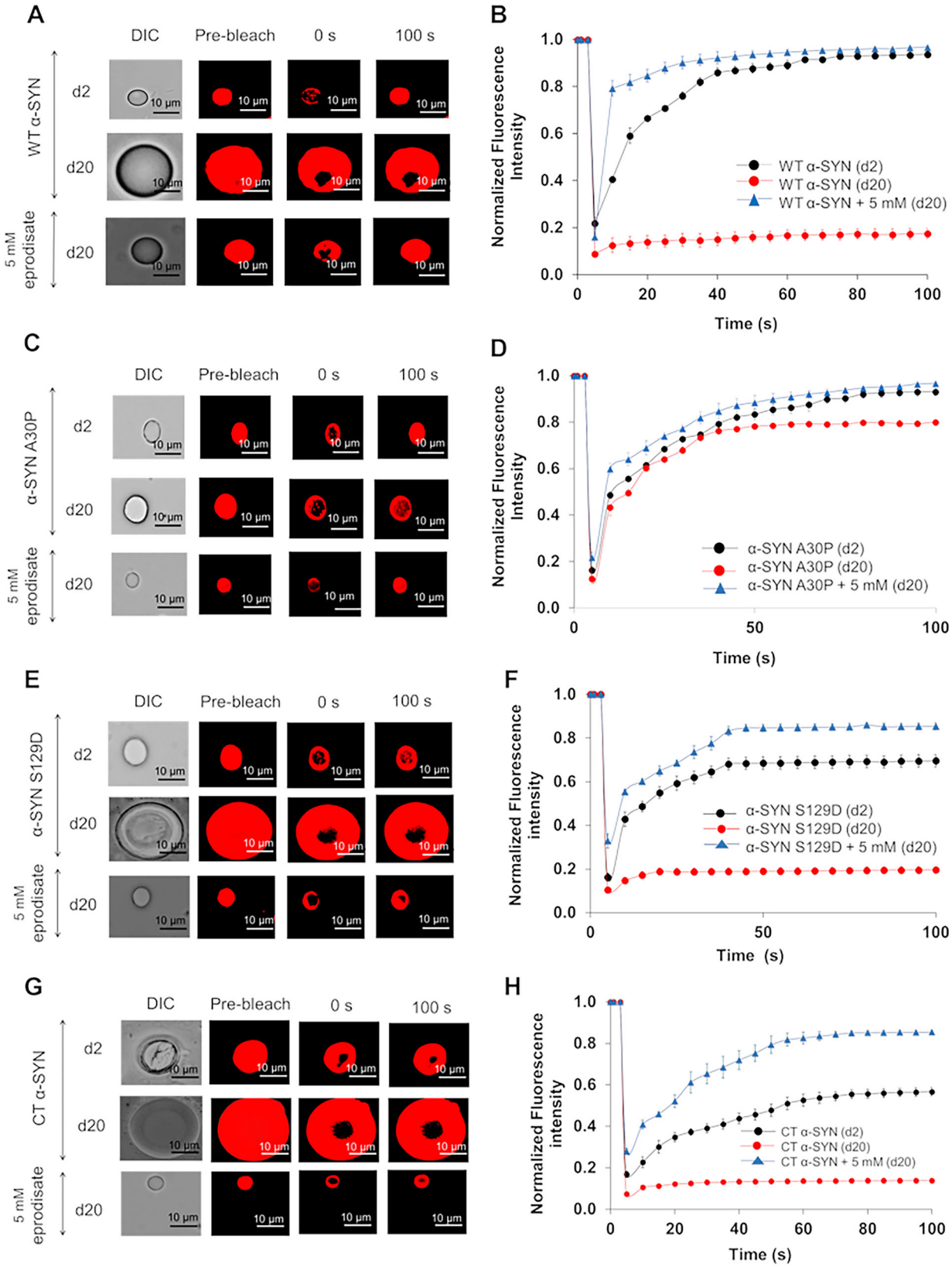

induced structural changes, suggesting that reduced WT α-SYN aggregation is due to delayed oligomer formation, consistent with the longer lag time (Fig. 6A). In case of A30P α-SYN (Fig. 7B) and S129D α-SYN (Fig. 7C), eprodisate showed marginal effect on the far UV CD spectra of the respective proteins. CT α-SYN (Fig. 7D) showed a pattern similar to WT α-SYN, with the most significant change in secondary structure occurring at the stage of oligomerisation in the presence of eprodisate. Thus, eprodisate induced order in the structure of WT α-SYN and CT α-SYN upon incubation, which reduced the final aggregation of these proteins in the presence of this GAG.

Fig. 8 | FRAP analysis of dynamics of phase-separated α-SYN variants. A, **B** WT α-SYN, (**C**, **D**) α-SYN A30P, (**E**, **F**) α-SYN S129D and (**G**, **H**) C-terminal truncated α-SYN (CT α-SYN) in the presence of eprodisate. α-SYN variants labeled with Rhodamine B exhibit red fluorescence. In each case, the left panel shows representative FRAP images of α-SYN droplets at the indicated time points (d2, d20) in the absence or presence of eprodisate, while the right panel shows the normalized FRAP curves of α-SYN droplets at d2, d20 and d20 with 5 mM eprodisate. The concentrations of α-SYN variants and eprodisate are 200 μM and 5 mM, respectively. In **B**, **D**, **F** and **H**, black circle with black dashed line represents protein alone at d2, red filled circle with red dashed line represents protein alone at d20 and a blue filled triangle with blue dashed line represents protein with 5 mM eprodisate at d20. All the experiments were carried out in the presence of 10% PEG8000. Line graphs are shown for mean ± sem of three independent replicates. Representative microscopy images are shown. Objective lens 100X, bar = 10 μm. Comparison of mobile fraction of α-SYN variants in the presence of eprodisate is shown in Supplementary Fig. 13. Source data are provided in Supplementary Data 1.

Fluorescence recovery after photobleaching

The dynamics of WT α-SYN and its variants within liquid droplets were investigated by fluorescence recovery after photobleaching (FRAP), utilizing droplets formed by rhodamine-labeled α-SYN variants. For WT α-SYN, FRAP analysis conducted immediately after droplet formation (d2) revealed nearly complete fluorescence recovery (Fig. 8A, B). The calculated mobile fraction was 92.1 ± 1.8% (Supplementary Fig. 13), suggesting that the protein was mobile and dynamic in its early phase of droplet formation. However, as the WT α-SYN droplets aged, significant reduction in fluorescence recovery was observed (Fig. 8A, B). At d20, the mobile fraction of WT α-SYN dropped significantly to 4.3 ± 1.2% (Supplementary Fig. 13). Reduced fluorescence recovery indicates decreased protein mobility and aggregation. The lower mobile fraction at d20 suggests altered droplet properties, likely becoming more rigid or gel-like due to WT α-SYN aggregation. In the presence of 5 mM eprodisate, faster fluorescence recovery of WT α-SYN droplet at d20 was observed (Fig. 8A, B), with almost complete recovery of mobile fraction (96.1 ± 0.3%) (Supplementary Fig. 13). This indicates that at higher concentration (5 mM), eprodisate reduces the amount of gel-like fraction of the protein inside the droplet. For the α-SYN A30P variant, droplets formed at d2 revealed fast fluorescence recovery (Fig. 8C, D), with the calculated mobile fraction being 92.0 ± 1.2% (Supplementary Fig. 13), similar to WT α-SYN. In case of aged α-SYN A30P droplets (d20), the mobile fraction inside the droplet increased to 78.3 ± 1.5% (Supplementary Fig. 13) which was higher than that observed for WT α-SYN. In the presence of 5 mM eprodisate, droplets formed by α-SYN A30P showed faster and higher fluorescence recovery at d20 as compared to untreated samples (Fig. 8C, D), with the mobile fraction being 95.3 ± 0.5% (Supplementary Fig. 13). On the other hand, for α-SYN S129D variant, FRAP analysis conducted immediately after droplet formation (d2) revealed a decrease in fluorescence recovery (Fig. 8E, F) as compared to WT α-SYN. The mobile fraction α-SYN S129D variant inside the droplet at d2 was calculated to be 64.3 ± 2.5% (Supplementary Fig. 13). The labeled protein recovered less and more slowly than WT α-SYN, indicating reduced molecular exchange and internal rearrangement. This suggests the α-SYN S129D variant forms more stable, less dynamic and less fluid droplets. In case of aged α-SYN S129D droplets (d20), significant reduction in the fluorescence recovery was seen (Figs. 8E, 8F), with the mobile fraction being 10 ± 1.2% (Supplementary Fig. 13). In the presence of 5 mM eprodisate, faster fluorescence recovery of α-SYN S129D droplet was observed at d20 (Fig. 8E, F) and the mobile fraction was 78.0 ± 1.5% (Supplementary Fig. 13). Similarly, in case of CT α-SYN, reduction in fluorescence recovery at d2 was observed (Fig. 8G-H) and the mobile fraction was the lowest (48.0 ± 1.2%) (Supplementary Fig. 13) among all variants. In case of aged CT α-SYN (d20), the mobile fraction was 7.0 ± 1.5% (Supplementary Fig. 13). In the presence of 5 mM eprodisate, fluorescence recovery of droplet at d20 was observed (Fig. 8G, H) and the mobile fraction was found to be 80.4 ± 1.3% (Supplementary Fig. 13). Eprodisate significantly enhances the fluorescence recovery of α-SYN variants inside the droplets (d20), indicating a faster dynamic behavior within these phase-separated structures. Taken together with fluorescence polarization and rheological studies, these findings indicate that eprodisate enhances molecular dynamics, promotes droplet fluidity and modulates α-SYN aggregation, highlighting its therapeutic potential in neurodegenerative diseases.

Effect of eprodisate on intracellular aggregation of WT α-SYN

To generate active seed, SH-SY5Y cells overexpressing WT α-SYN were incubated with exogenously produced recombinant human WT α-SYN, producing visible inclusions after 72 h[61]. After five days of incubation, addition of α-SYN significantly promoted inclusion formation in stably overexpressing SH-SY5Y cells (Fig. 9A), with over 60% of cells showing fluorescent puncta (Fig. 9B). These inclusions were distributed throughout the cytoplasm as large irregular foci and small puncta. Aggregation also increased oxidative stress, with ROS levels rising by over 40% compared to untreated cells (Fig. 9C).

Treatment with 5 mM eprodisate reduced WT α-SYN-positive aggregates by ~35% compared to untreated control (Fig. 9A). Aggregation decreased in a concentration-dependent manner (Fig. 9B), accompanied by reduced ROS levels (Fig. 9C). α-SYN aggregation reduced cell viability by ~44% (Fig. 9D), while eprodisate improved viability to ~75%, indicating a cytoprotective effect.

Conclusion

Eprodisate, a glycosaminoglycan mimetic, has been shown to be well-tolerated for clinical applications. In this work, we show that the molecule inhibited phase separation and attenuated gel formation by α-SYN in a concentration-dependent manner. Eprodisate proved to be a suitable inhibitor for all four disease-relevant variants of α-SYN. Notably, aggregation of all α-SYN variants was enhanced in the presence of chondroitin sulphate. Eprodisate was able to inhibit aggregation of these proteins in this case as well. The molecule seems to work by reducing droplet fusion and biomolecular condensation of the protein. This slows down the transition from liquid-like viscous behavior to elastic-solid-like gel formation by the variants (Fig. 10). This was also suggested by increased mobility of the variant proteins in the droplets and their reduced polarization in the presence of eprodisate. Eprodisate was successful in inhibiting aggregation of WT α-SYN in a cell model of synucleinopathy and improved cell survival. Thus, therapeutic efficacy of eprodisate can be explored further in higher PD models.

Materials

1,3-Propanedisulphonic acid disodium salt (eprodisate), luria-bertani (LB) broth, lysozyme from chicken egg white, ampicillin, sodium azide, thioflavin T, thioflavin S, geneticin (G418), bicinchoninic acid (BCA), PEG8000, rabbit polyclonal FITC conjugated antibody (F0382; 1:5000 dilution), Dulbecco's modified Eagle's medium (DMEM), trypsin–EDTA solution (0.25% w/v), penicillin–streptomycin antibiotic, fluorescein isothiocyanate (FITC) and rhodamine B were purchased from Sigma-Aldrich Chemicals Pvt. Ltd. Bengaluru, India. Rabbit monoclonal anti-alpha-SYN antibody (MJFR1, ab13850, 1.134 mg/mL, 1:3000) was a product of Abcam and was purchased from Nulife Consultants & Distributors Pvt. Ltd., New Delhi, India. The antibody was used following the manufacturer's recommendation at 1:3000 dilution. Abcam has confirmed its specificity, as demonstrated by the absence of signal in *SNCA* knockout cells. This antibody recognizes an epitope spanning amino acids 118–123 of α-SYN. The rabbit polyclonal α-SYN (1–10 amino acids) targets an N-terminal epitope, which remains present in the CT α-SYN species[62]. Fetal bovine serum (FBS), Ham's F-12 (Kaighn's, F-12K), opti-MEM reduced serum medium, lipofectamine 3000, P3000 and MTT (3-(4,5-dimethylthiazol-2-yl)-2,5-diphenyltetrazolium bromide) were purchased from Invitrogen Corporation, California, USA.

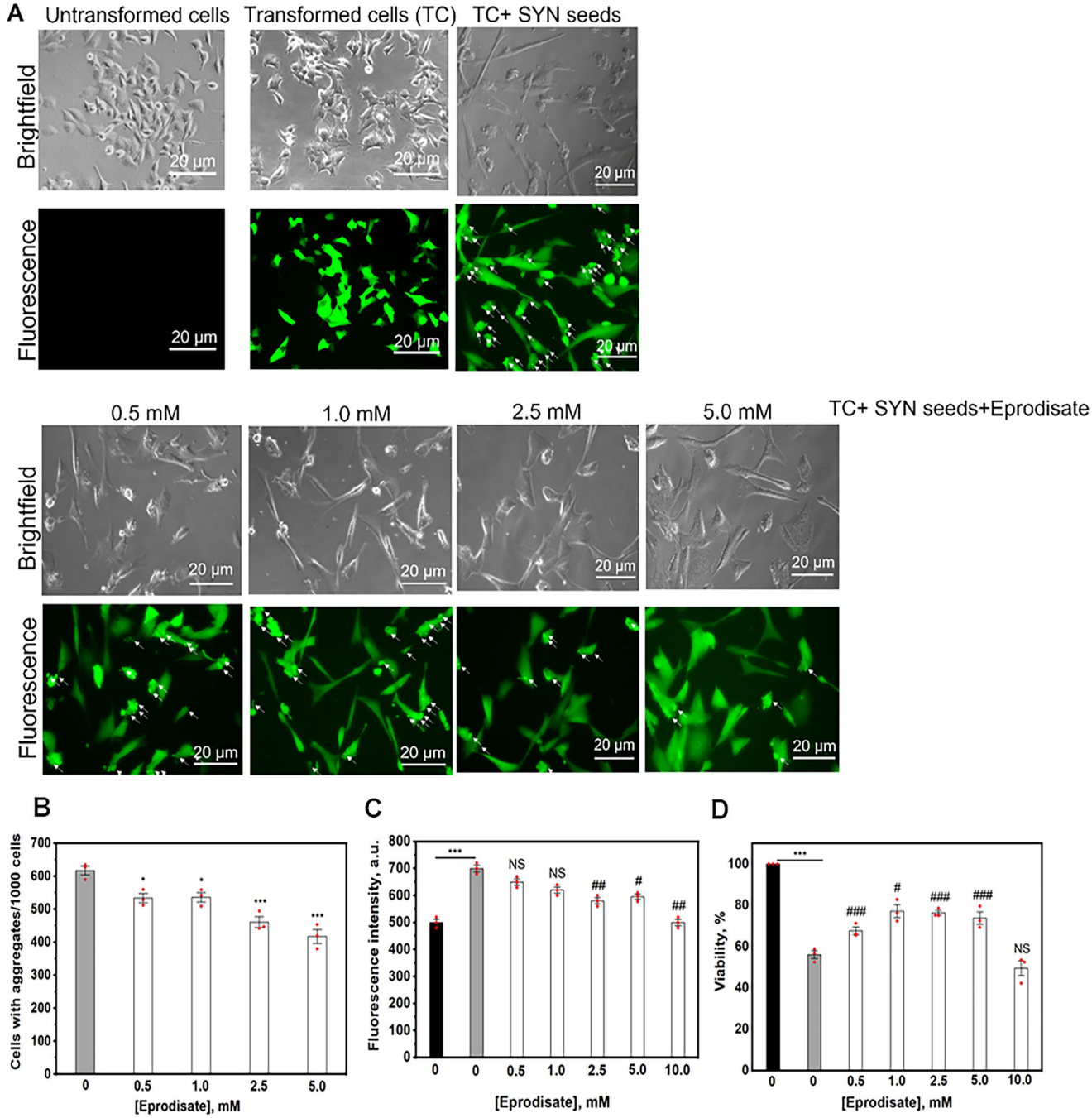

Dialysis membrane (snakeskin membrane, MWCO 3.5 kDa) was purchased from Thermo Fisher Scientific, Mumbai, India. Chondroitin sulphate (Grade A) was purchased from HiMedia Laboratories Pvt. Ltd., Mumbai, India. DEAE-Sepharose matrix was from GE Healthcare, Uppsala, Sweden. Nitrocellulose membrane (0.45 μm) was a product of Global Life Sciences Solutions Operations UK Ltd. and purchased by Hyclone Life Sciences Solutions India Pvt. Ltd. QIAEX II gel extraction kit was purchased from Qiagen India Pvt. Ltd., New Delhi. SH-SY5Y neuroblastoma cell lines were purchased from National Cell Repository, National Centre for Cell Science (NCCS), Pune, India (STR loci match with ATCC STR profile database: 100%). The cell line is not listed as a commonly misidentified cell line by the International Cell Line Authentication Committee (ICLAC). Cells were received as mycoplasma-free and were used at low passage numbers (<35) to ensure phenotypic consistency. All other reagents and chemicals were of analytical grade or higher.

Methods

Site-directed mutagenesis of wild-type α-SYN to α-SYN variants (A30P, S129D, CT)

Site-directed mutagenesis was performed to create different mutants of *α-SYN* using polymerase chain reaction (PCR) and subsequent *Dpn*I digestion for selection of mutants. The template DNA used for the PCR reaction was a construct of pRSETB vector containing the insert of *α-SYN*[41]. Primers were designed using Primer3 (v.0.4.0) software[63]. Mutations were confirmed by DNA sequencing.

For amplification of *α-SYN A30P* mutant, forward primer: 5' GTGTGGCAGAAGCA*CCA*GGAAAGACAAAAGAG 3' (the italicized and underlined sequences denote site of mutation) and reverse primer: 5' CTCTTTTGTCTTTCC*TGG*TGCTTCTGCCACAC 3' were used.

For amplification of *α-SYN S129D* mutant, forward primer: 5' CTTATGAAATGCCT*GAT*GAGGAAGGGTATC 3' (the italicized and

Fig. 9 | Effect of eprodisate on exogenous α-SYN induced aggregation in SH-SY5Y cells overexpressing wild type α-SYN (WT α-SYN). A Microscopy images were recorded in the presence of different concentrations of eprodisate after incubation for 5 days. Arrows indicate localized green fluorescence of EGFP-α-SYN aggregates. Transformed cells indicate cells overexpressing WT α-SYN in the absence of exogenous seeds. Cells were visualized under the 40X objective. Bar = 20 µm. **B** Quantitative measurement of cells exhibiting fluorescent puncta after 5 days post addition of α-SYN in the absence (gray bars) and presence of eprodisate (empty bars). Cells (1000 in each case) were counted across 10 fields. $^{*}p < 0.05$, NS=non-significant against α-SYN treated cells in the absence of eprodisate. *p*– values for α-SYN treated cells with 0.5 mM eprodisate ($^{*}p = 0.0132$), α-SYN treated cells with 1.0 mM eprodisate ($^{*}p = 0.0161$), α-SYN treated cells with 2.5 mM eprodisate ($^{***}p = 0.0020$) and α-SYN treated cells with 5.0 mM eprodisate ($^{***}p = 0.0014$) are calculated with respect to α-SYN treated cells in the absence of eprodisate. **C** Effect of eprodisate on oxidative stress. SH-SY5Y cells stably expressing EGFP-α-SYN were incubated in the absence of exogenous α-SYN and eprodisate (black bar), absence of small molecule (gray bar) and presence of exogenous α-SYN and eprodisate (empty bars) and oxidative stress was measured by dihydroethidium (DHE) dye after 5 days. $^{***}p < 0.001$ against cells incubated in the absence of exogenous α-SYN and eprodisate, $^{\#\#}p < 0.001$, $^{\#}p < 0.05$, NS non-significant against cells incubated in the presence of exogenous α-synuclein and absence eprodisate. *p*– values for α-SYN treated cells with 0.5 mM eprodisate (NS = 0.0051), α-SYN treated cells with 1.0 mM eprodisate (NS = 0.0080), α-SYN treated cells with 2.5 mM eprodisate ($^{\#\#}p = 0.0080$), α-SYN treated cells with 5.0 mM eprodisate ($^{\#}p = 0.0375$) and α-SYN treated cells with 10.0 mM eprodisate ($^{\#\#}p = 0.0025$) are calculated with respect to α-SYN treated cells in the absence of eprodisate. Values shown are mean ± sem of three independent experiments and analyzed by one-way Analysis of Variance (ANOVA) for multiple comparisons. **D** SH-SY5Y cells stably expressing EGFP-α-SYN were incubated in the absence of exogenous α-SYN and eprodisate (black bars), absence of small molecule (gray bar) and presence of exogenous α-SYN and eprodisate (empty bars) and viability was measured by MTT assay after 5 days. The viability of cells incubated in the absence of exogenous α-SYN and eprodisate for 5 days was assigned an arbitrary value of 100%. $^{***}p < 0.001$ against cells incubated in the absence of exogenous α-SYN and eprodisate, $^{\#\#\#}p < 0.001$, $^{\#}p < 0.05$, NS non-significant against cells incubated in the presence of exogenous α-synuclein and absence eprodisate. *p*– values for α-SYN treated cells with 0.5 mM eprodisate ($^{\#}p = 0.0115$), α-SYN treated cells with 1.0 mM eprodisate ($^{\#\#\#}p = 0.0041$), α-SYN treated cells with 2.5 mM eprodisate ($^{\#\#\#}p = 0.0007$), α-SYN treated cells with 5.0 mM eprodisate ($^{\#\#\#}p = 0.0075$) and α-SYN treated cells with 10.0 mM eprodisate (NS = 0.1780) are calculated with respect to α-SYN treated cells in the absence of eprodisate. Values shown are mean ± sem of three independent experiments and analyzed by one-way Analysis of Variance (ANOVA) for multiple comparisons. Source data are provided in Supplementary Data 1.

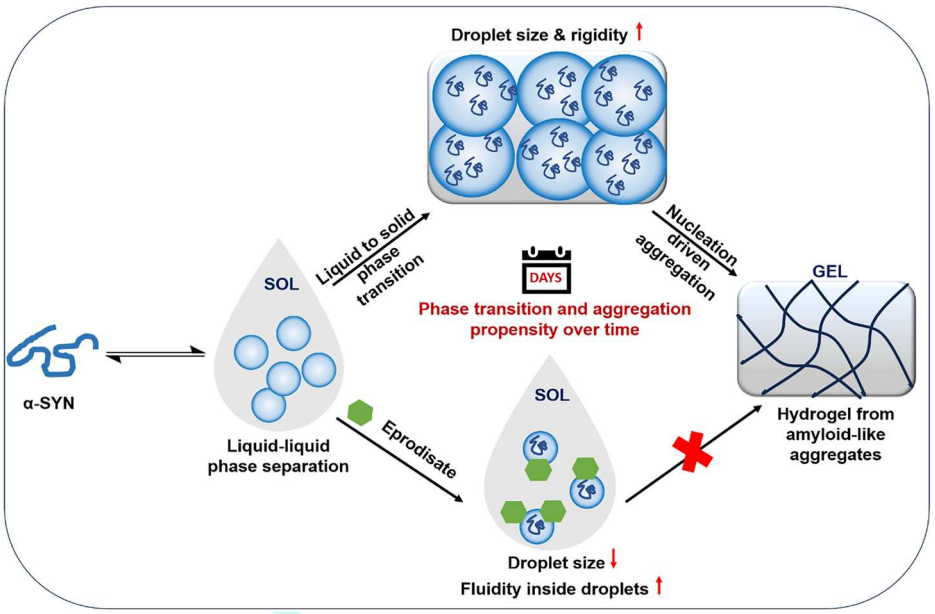

Fig. 10 | Scheme illustrating mechanism of action of eprodisate on phase transition and amyloid aggregation of α-SYN variants used in this study. α-SYN, in its monomeric state, undergoes liquid–liquid phase transition from a soluble form (sol) to a more structured gel-like state inside droplets. These droplets are dynamic and soft, held together by weak, reversible interactions between monomeric α-SYN molecules. Over time, the droplets mature and coalesce, strengthening into a hydrogel—an organized, highly cross-linked network, further causing the formation of amyloid fibrils, leading to neurodegeneration. Eprodisate works by reducing the size of liquid droplets and the overall biomolecular condensation of α-SYN, thus preventing the protein from undergoing the sol-to-gel transition. This inhibitory effect helps to maintain the α-SYN droplets in a less aggregated, more dynamic state, reducing the risk of aggregation and potentially alleviating pathologies associated with protein misfolding, such as Parkinson's disease.

underlined sequences denote site of mutation) and reverse primer: 5' GATACCCTTCCTC*ATC*AGGCATTTCATAAG 3' were used.

For amplification of *α-SYN C-T* mutant, forward primer: 5' *GGG*CATATGATGGATGTATTCATGAAAGG 3' (the restriction site of *Nde*I is bold and underlined while overhangs are italicized) and reverse primer: 5' *GG*GCTAGCAGGATCCACAGGCATATCTTCC 3' (the restriction site of *Nhe*I is bold and underlined while overhangs are italicized) were used. *CT α-SYN* codes for C-terminal truncated α-SYN (1-120 aa), the predominant toxic species found in Lewy bodies[64,65]. The amplified *CT α-SYN* insert was cloned into pRSETB by deleting the full-length *α-SYN* gene using *Nde*I and *Nhe*I. Gel-purified backbone and insert were ligated using T4 DNA ligase at 16 °C for 16 h. The ligation mixture was used to transform competent *E. coli* DH5α cells and was plated on LB agar plate containing ampicillin (60 µg/mL). Plasmids were isolated from colonies by alkaline lysis method and were confirmed by PCR and restriction digestion with *Nde*I and *Nhe*I.

Purification of human recombinant α-SYN variants

E. coli BL21 (DE3) cells were transformed with pRSETB plasmid carrying genes for *α-SYN* variants. Briefly, transformed *E. coli* BL21 (DE3) cells were grown in LB_{amp} medium at 37 °C till A_{600} 0.6. Cells were induced to express recombinant human α-SYN variant proteins with 1 mM IPTG for 4 h. Following cell lysis, the pH of the lysates (labeled as lysate 1) was reduced to 3.5 with 1 N HCl and incubated for 10 min for precipitation of contaminating proteins. The lysates were centrifuged, and the pH of the supernatants was raised to 7.5 (labeled as lysate 2)[11,41]. Recombinant human α-SYN variant proteins were purified by anion exchange chromatography using DEAE-Sepharose, dialyzed and lyophilized.

Liquid–liquid phase separation (LLPS)

Purified recombinant human α-SYN variant proteins were suspended in 20 mM Tris HCl, pH 7.8, containing 0.02% sodium azide (stock solution 484 µM). Reaction mixture of proteins (200 µM + 10% PEG 8000) was prepared

in a total volume of 200 µL in the absence and presence of different concentrations of eprodisate. An aliquot (5 µL) of each sample was pipetted out, drop-casted onto glass slides with a 12 mm coverslip and the sides of the coverslips were sealed with commercially available nail-paint[13]. The slides were kept in a moist chamber at 37 °C for subsequent incubation periods and phase-separated droplets were visualized with 100× oil immersion objective in the DIC (differential interference contrast) mode under Nikon Eclipse E600 microscope.

Rhodamine staining

For labeling WT α-SYN and its variants, in brief, 10X molar excess of rhodamine (dissolved in DMSO) was added to α-SYN variants and was incubated for 4 h at room temperature (RT) followed by 6 h at 4 °C with slow mixing with the help of a magnetic bead. The excess dye was removed by dialysis against 20 mM Tris HCl (pH 7.8) at 4 °C for 72 h with a change of buffer every 5 h. Reaction mixture of rhodamine labeled α-SYN variants (200 µM + 10% PEG8000) was prepared in a total volume of 200 µL in the absence and presence of different concentrations of eprodisate. An aliquot (10 µL) of each sample was pipetted out, drop-casted onto glass slides with a 12 mm coverslip and slides of the coverslips were sealed with commercially available nail-paint[13]. The slides were kept in a moist chamber at 37 °C for subsequent incubation periods till day 20 and phase-separated droplets were visualized with 100× oil immersion objective in the fluorescence mode under Nikon Eclipse E600 microscope.

Thioflavin S (ThioS) staining

ThioS (stock solution 250 µM) was prepared in 20 mM Tris-HCl buffer, pH 7.8. Reaction mixture (200 µM protein + 10% PEG8000, 9 µL) was mixed with 20 µM ThioS dye (1 µL) and incubated at 37 °C for different time intervals. Fluorescence intensity of ThioS was visualized using 100× oil immersion objective and 10× eyepiece in the DIC mode using Nikon Eclipse E600 microscope.

Transmission electron microscopy

WT α-SYN solution (monomer, droplets or fibrils) was drop-cast on a carbon-coated copper grid, allowed to dry in air and negatively stained with 2% uranyl acetate. The grids were subjected to transmission electron microscopy (TEM) imaging (TF20, FEI, USA) at 200 kV and 6600× magnification[66].

Rheological measurements

Rheological measurements were performed on Anton Paar Rheometer MCR 302 equipped with Rheocompass software using parallel plate (PP-25) geometry at a measuring distance of 0.5 mm at 37 °C. To prevent solvent evaporation during extended experiments, a solvent trap was used to cover the measuring plate area for all measurements. Frequency sweep oscillatory rheology was performed from 0.1 to 100 rad/s at a constant 0.05% strain in the linear viscoelastic region and amplitude sweep studies were performed from 0.01% to 100% strain at 10 rad/s to determine the crossover point. Samples were prepared by incubating α-SYN variants at 37 °C in the presence/absence of different concentrations of eprodisate for 0, 5, and 20 days. The storage moduli and loss moduli obtained from the above experiments (denoted by G' and G'', respectively) were utilized to calculate the damping factor $\tan\delta = G''/G'$ as a numerical indicator for elastic and viscous behavior.

Fluorescence polarization

For labeling of proteins, 10X molar excess of FITC (dissolved in DMSO) was added to α-SYN variants[46]. Each mixture was incubated for 4 h at room temperature, followed by 6 h at 4 °C with slow mixing with the help of a magnetic bead. Excess dye was removed by dialysis. The FITC-labeled protein was diluted into a solution of unlabeled protein (1:99 molar ratio) to achieve a final protein concentration of 100 µM and incubated in the absence and presence of different concentrations of eprodisate. Before measurement, samples were diluted to 10 µM. All FP measurements were recorded using a microplate reader (Cytation 5, BioTek) equipped with excitation (485 ± 20 nm) and emission (535 ± 25 nm) filters for FITC fluorescence.

Thioflavin T (ThT) assay

Purified recombinant human α-SYN variant proteins (7 mg/mL, 20 mM Tris-HCl, pH 7.8 containing 0.02% sodium azide) were incubated in the absence and presence of different concentrations of eprodisate and absence or presence of PEG at 37 °C. The proteins were also incubated in the presence of chondroitin sulfate (CSA, 1 mM, in 20 mM Tris-HCl, pH 7.8). The molar extinction coefficients used for calculating the concentration of WT α-SYN, α-SYN A30P, and α-SYN S129D were 5800 M^{-1} cm^{-1}[67] and for α-SYN CT were 1400 M^{-1} cm^{-1}[68]. Aliquots were withdrawn at regular intervals, and the extent of aggregation was analyzed by Thioflavin T fluorescence spectroscopy (λ_{ex} 440 nm, λ_{em} 485 nm). Aggregation kinetics was followed by fitting the data using the formula[66,69],

$$y = y_i + mx_i + \frac{y_f + mx_f}{1 + e^{\frac{x - x_0}{\tau}}}$$

where x_0 is the midpoint of maximum signal. Initial baseline in the lag phase is described by $y_i + mx_i$ whereas the final baseline upon completion of the growth phase is described by $y_f + mx_f$. The apparent rate constant (k_{app}) is $1/\tau$ and lag time is calculated to be $x_0 - 2\tau$.

Circular dichroism spectroscopy

Far-UV circular dichroism (CD) spectra of recombinant human α-SYN variant proteins (5 µM) incubated in the absence and presence of different concentrations of eprodisate were recorded on a spectropolarimeter (J-815, Jasco) in the wavelength range of 200–240 nm using a cuvette with 0.1 cm path-length. The average of three scans was recorded for each spectrum and the spectrum of buffer was subtracted from that of the protein.

Fluorescence recovery after photobleaching (FRAP)

For in vitro FRAP study, α-SYN variants (200 µM) were allowed to phase separate in the presence of 10% PEG8000 for two time points, viz. d2 and d20. All the reaction mixtures contained 10% labeled α-SYN variants (labeled with Rhodamine B) and 90% unlabeled protein[13]. The solutions were spotted onto 15 mm depression slides and sandwiched with an 18 mm coverslip followed by sealing of the edges of the coverslip with commercially available nail-paint. After confirmation of droplet formation by fluorescence microscopy (Nikon Eclipse E600), the slides containing the droplets were subjected to FRAP using a laser-scanning confocal microscope (Zeiss LSM880 microscope) with a 100× oil immersion objective. The FRAP experiment was also performed in the presence of 5 mM eprodisate at d20 of incubation. Photo-bleaching of the phase-separated droplets of α-SYN variants was carried out using a 561 nm DPSS 561-10 laser at the fifth cycle and recovery was recorded till the fluorescence emission reached a plateau. Regions of interest (ROIs) were manually defined as areas (4–5 µm in diameter) within individual, spherical droplets. Intensities from three different ROIs: actual bleaching region (ROI-1), reference region on the same droplet but at a different location to correct for passive bleaching during laser exposure (ROI-2) and a region outside the droplet to correct for background fluorescence intensity (ROI-3), were measured. Only well-isolated droplets with uniform pre-bleach fluorescence intensity were selected to avoid edge effects or signal overlap. The selected ROI-1 was bleached with 100% laser power. All the measurements were performed at room temperature and at least in triplicate. After acquiring three images before bleaching, recovery was monitored for ~100 s with time interval of 5 s. The images were corrected for laser bleaching by selecting a fluorescent region outside the ROI. The mobility fraction (R) was calculated using the formula, $R = (F_\infty - F_0)/(F_i - F_0)$, where F_∞ = fluorescence in the ROI after full recovery,

F_i = fluorescence in the ROI prior to bleaching, and F_0 = fluorescence in the ROI just after photobleaching.

Aggregation of WT α-SYN in SH-SY5Y cells

SH-SY5Y cells were transfected with pEGFP-*α-SYN* following a standard protocol[70]. Complete DMEM/F-12 medium (1% penicillin–streptomycin, 10% FBS) (3 mL) was seeded with 2.5×10^5 cells in a six-well plate and incubated for 24 h. Transfection was performed with 3 μg DNA (pEGFP-*α-SYN*) using Lipofectamine™ 3000 according to the manufacturer's protocol. Transformed cells were grown up to 70–80% confluency in T 25 flasks. Cells were trypsinized, seeded at 40,000 cells/mL in 24-well plates and incubated in the presence of complete media for 24 h at 37 °C with 5% CO_2. After washing twice with PBS, complete medium supplemented with purified recombinant human α-SYN along with different concentrations of eprodisate. The cells were further incubated up to six days for induction of intracellular aggregation. Aggregation of WT α-SYN was observed under a fluorescence microscope (Nikon Eclipse Ti) using 40× objective lens.

Analysis of intracellular reactive oxygen species (ROS)

The generation of reactive oxygen species (ROS) was measured using dihydroethidium (DHE)[71]. Briefly, DHE (5 μM) was dissolved in complete media and incubated with 40,000 cells/well in a 96-well plate for 1 h at 37 °C. Emission intensity was recorded at 610 nm after exciting the samples at 518 nm, using a microplate reader (Synergy H1 multi-mode, BioTek). The emission intensity of DHE alone was subtracted as blank.

Cell viability assay

The viability of cells was measured using MTT[72]. Cells were grown to 70–80% confluency, trypsinized, and 40,000 cells/well were seeded in a 96-well plate and incubated with exogenous α-SYN and eprodisate for 5 days. Following this, the cells were incubated with MTT solution (5 mg/mL in DMEM) for 4 h at 37 °C, 5% CO_2. After removal of the medium and MTT, purple formazan crystals were dissolved by the addition of DMSO for 2 h at room temperature. The absorbance of dissolved formazan was recorded at 570 nm using a microplate reader (Synergy H1, BioTek).

Statistical analysis

Statistical analysis was performed with the help of GraphPad Prism 8 software. Results were expressed as a mean ± SEM. One-way analysis of variance (ANOVA) was used to compare the statistical significance across protein variants, and Tukey's multiple comparison test was used for post-hoc analysis. $p < 0.05$ was considered statistically significant.

Reporting summary

Further information on research design is available in the Nature Portfolio Reporting Summary linked to this article.

Data availability

The authors declare that all data supporting the findings of this study are available within the paper and its supplementary information file. These data are also available upon request from the corresponding author. Source data for the figures and supplementary information file are provided in Supplementary Data 1.

Received: 6 June 2025; Accepted: 9 April 2026;
Published online: 27 April 2026

References

1. Dignon, G. L., Zheng, W., Kim, Y. C. & Mittal, J. Temperature-controlled liquid-liquid phase separation of disordered proteins. *ACS Cent. Sci.* **5**, 821–830 (2019).
2. Fonin, A. V. et al. Biological soft matter: Intrinsically disordered proteins in liquid-liquid phase separation and biomolecular condensates. *Essays Biochem.* **66**, 831–847 (2022).
3. Dao, T. P. et al. Ubiquitin modulates liquid-liquid phase separation of UBQLN2 via disruption of multivalent interactions. *Mol. Cell* **69**, 965–978 (2018).
4. Dignon, G. L., Best, R. B. & Mittal, J. Biomolecular phase separation: From molecular driving forces to macroscopic properties. *Annu. Rev. Phys. Chem.* **71**, 53 (2020).
5. Burré, J., Sharma, M. & Südhof, T. C. Alpha-Synuclein assembles into higher-order multimers upon membrane binding to promote SNARE complex formation. *Proc. Natl. Acad. Sci. USA* **111**, E4274–E4283 (2014).
6. Deleersnijder, A., Gerard, M., Debyser, Z. & Baekelandt, V. The remarkable conformational plasticity of alpha-synuclein: blessing or curse? *Trends Mol. Med.* **19**, 368–377 (2013).
7. Longhena, F., Faustini, G., Spillantini, M. G. & Bellucci, A. Living in promiscuity: the multiple partners of alpha-synuclein at the synapse in physiology and pathology. *Int. J. Mol. Sci.* **20**, 141 (2019).
8. Ejma, M. et al. The links between Parkinson's disease and cancer. *Biomedicines* **8**, 416 (2020).
9. Patel, A. et al. A liquid-to-solid phase transition of the ALS protein FUS accelerated by disease mutation. *Cell* **162**, 1066–1077 (2015).
10. Babinchak, W. M. & Surewicz, W. K. Liquid–liquid phase separation and its mechanistic role in pathological protein aggregation. *J. Mol. Biol.* **432**, 1910–1925 (2020).
11. Kardani, J. & Roy, I. Understanding caffeine's role in attenuating the toxicity of α-synuclein aggregates: Implications for risk of Parkinson's Disease. *ACS Chem. Neurosci.* **6**, 1613–1625 (2015).
12. Panuganti, V. & Roy, I. Oligomers, fibrils and aggregates formed by alpha-synuclein: Role of solution conditions. *J. Biomol. Struct. Dyn.* **40**, 4389–4398 (2022).
13. Ray, S. et al. Alpha-Synuclein aggregation nucleates through liquid-liquid phase separation. *Nat. Chem.* **12**, 705–716 (2020).
14. de Oliveira, G. A. P., Cordeiro, Y., Silva, J. L. & Vieira, T. C. R. G. Liquid-liquid phase transitions and amyloid aggregation in proteins related to cancer and neurodegenerative diseases. *Adv. Protein Chem. Struct. Biol.* **118**, 289–331 (2019).
15. Mukherjee, S., Poudyal, M., Dave, K., Kadu, P. & Maji, S. K. Protein misfolding and amyloid nucleation through liquid-liquid phase separation. *Chem. Soc. Rev.* **53**, 4976–5013 (2024).
16. Hardenberg, M. C. et al. Observation of an α-synuclein liquid droplet state and its maturation into Lewy body-like assemblies. *J. Mol. Cell Biol.* **13**, 282–294 (2021).
17. Walker, D. G. et al. Changes in properties of serine 129 phosphorylated α-synuclein with progression of Lewy-type histopathology in human brains. *Exp. Neurol.* **240**, 190–204 (2013).
18. Games, D. et al. Reducing C-terminal-truncated alpha-synuclein by immunotherapy attenuates neurodegeneration and propagation in Parkinson's disease-like models. *J. Neurosci.* **34**, 9441–9454 (2014).
19. Huang, S. et al. -Synuclein phase separation and amyloid aggregation are modulated by C-terminal truncations. *FEBS Lett.* **596**, 1388–1400 (2022).
20. Suthar, S. K. & Lee, S. Y. Truncation or proteolysis of alpha-synuclein in Parkinsonism. *Ageing Res. Rev.* **90**, 101978 (2023).
21. Amagai, R. et al. C-terminal truncation is a prominent post-translational modification of human erythrocyte alpha-synuclein. *J. Biochem.* **175**, 649–658 (2024).
22. Li, J. F. et al. Curcumin inhibits α-synuclein aggregation by acting on liquid–liquid phase transition. *Foods* **13**, 1287 (2024).
23. Febbraro, F. et al. Ser129D mutant alpha-synuclein induces earlier motor dysfunction while S129A results in distinctive pathology in a rat model of Parkinson's disease. *Neurobiol. Dis.* **56**, 47–58 (2013).
24. Xu, B. et al. Distinct effects of familial Parkinson's disease-associated mutations on α-synuclein phase separation and amyloid aggregation. *Biomolecules* **13**, 726 (2023).
25. Conway, K. A. et al. Acceleration of oligomerization, not fibrillization, is a shared property of both α-synuclein mutations linked to early-onset

Parkinson's disease: Implications for pathogenesis and therapy. *Proc. Natl. Acad. Sci. USA* **97**, 571–576 (2000).
26. Fredenburg, R. A. et al. The impact of the E46K mutation on the properties of α-synuclein in its monomeric and oligomeric states. *Biochemistry* **46**, 7107–7118 (2007).
27. Parui, A., Biswas, S. & Roy, I. Meclofenoxate inhibits aggregation of alpha-synuclein in vitro. *Protein Pept. Lett.* **30**, 361–366 (2023).
28. Dada, S. T. et al. Pharmacological inhibition of α-synuclein aggregation within liquid condensates. *Nat. Commun.* **15**, 3835 (2024).
29. Perry, G. et al. Basic fibroblast growth factor binds to filamentous inclusions of neurodegenerative diseases. *Brain Res.* **579**, 350–352 (1992).
30. van Horssen, J. et al. Absence of heparan sulfate proteoglycans in Lewy bodies and Lewy neurites in Parkinson's disease brains. *J. Alzheimers Dis.* **6**, 469–474 (2004).
31. Cohlberg, J. A., Li, J., Uversky, V. N. & Fink, A. L. Heparin and other glycosaminoglycans stimulate the formation of amyloid fibrils from alpha-synuclein in vitro. *Biochemistry* **41**, 1502–1511 (2002).
32. Maïza, A. et al. The role of heparan sulfates in protein aggregation and their potential impact on neurodegeneration. *FEBS Lett.* **592**, 3806–3818 (2018).
33. Li, Y. et al. Copper and iron ions accelerate the prion-like propagation of α-synuclein: A vicious cycle in Parkinson's disease. *Int. J. Biol. Macromol.* **163**, 562–573 (2020).
34. Stopschinski, B. E. et al. Specific glycosaminoglycan chain length and sulfation patterns are required for cell uptake of tau versus α-synuclein and β-amyloid aggregates. *J. Biol. Chem.* **293**, 10826–10840 (2018).
35. Tao, Y. et al. Heparin induces alpha-synuclein to form new fibril polymorphs with attenuated neuropathology. *Nat. Commun.* **13**, 4226 (2022).
36. Rumjon, A., Coats, T. & Javaid, M. M. Review of eprodisate for the treatment of renal disease in AA amyloidosis. *Int. J. Nephrol. Renovasc. Dis.* **5**, 37–43 (2012).
37. Manenti, L., Tansinda, P. & Vaglio, A. Eprodisate in amyloid A amyloidosis: a novel therapeutic approach? *Expert Opin. Pharmacother.* **9**, 2175–2180 (2008).
38. Wang, P. & Ding, K. Proteoglycans and glycosaminoglycans in misfolded proteins formation in Alzheimer's disease. *Protein Pept. Lett.* **21**, 1048–1056 (2014).
39. Thorne, J. et al. Serum amyloid A protein-associated kidney disease: Presentation, diagnosis, and management. *Kidney Med.* **4**, 100504 (2022).
40. Dember, L. M. et al. Eprosidate for the treatment of renal disease in AA amyloidosis. *N. Engl. J. Med.* **356**, 2349–2360 (2007).
41. Cappai, R. et al. Dopamine promotes α-synuclein aggregation into SDS-resistant soluble oligomers via a distinct folding pathway. *FASEB J.* **19**, 1377–1379 (2005).
42. Xu, B., Chen, J. & Liu, Y. Curcumin interacts with α-synuclein condensates to inhibit amyloid aggregation under phase separation. *ACS Omega* **7**, 30281–30290 (2022).
43. Xu, B., Mo, X., Chen, J., Yu, H. & Liu, Y. Myricetin inhibits α-synuclein amyloid aggregation by delaying the liquid-to-solid phase transition. *Chembiochem* **23**, e202200216 (2022).
44. Darling, A. L. & Shorter, J. Combating deleterious phase transitions in neurodegenerative disease. *Biochim. Biophys. Acta Mol. Cell Res.* **1868**, 118984 (2021).
45. Voorhees, P. W. The theory of Ostwald ripening. *J. Stat. Phys.* **38**, 231–252 (1985).
46. Haney, C. M. et al. Site-specific fluorescence polarization for studying the disaggregation of α-synuclein fibrils by small molecules. *Biochemistry* **56**, 683–691 (2017).
47. Luk, K. C., Hyde, E. G., Trojanowski, J. Q. & Lee, V. M. Y. Sensitive fluorescence polarization technique for rapid screening of α-synuclein oligomerization/fibrillization inhibitors. *Biochemistry* **46**, 12522–12529 (2007).
48. Johansson, L. B. A. Limiting fluorescence anisotropies of perylene and xanthene derivatives. *J. Chem. Soc. Trans.* **86**, 2103–2107 (1990).
49. Joseph, J. P. et al. Unraveling on-demand strain-stiffening in nanofibrous peptide–polymer conjugates to mimic contractility in actinomyosin networks. *Chem. Mater.* **34**, 4364–4374 (2022).
50. Mavlankar, N. A. et al. Maneuvering mineralization of self-assembled peptide nanofibers for designing mechanically-stiffened self-healable composites toward bone-mimetic ECM. *J. Mater. Chem. B* **12**, 8688–8701 (2024).
51. Nath, D., Ralhan, J., Joseph, J. P., Miglani, C. & Pal, A. Thermoresponsive injectable hydrogel to mimic the heat and strain-stiffening behaviour of biopolymers toward muscle cell proliferation. *Biomacromolecules* **25**, 853–863 (2024).
52. Mavlankar, N. A., Awasthi, A. K., Ralhan, J. & Pal, A. Amyloid-inspired peptide self-assembly/disassembly as intervened by gold nanoparticles and polydopamine coating to dictate spatiotemporal organization. *ChemNanoMat* **8**, e202200368 (2022).
53. Cofelice, M., Messia, M. C., Marconi, E., Cuomo, F. & Lopez, F. Effect of the xanthan gum on the rheological properties of alginate hydrogels. *Food Hydrocolloids* **142**, 108768 (2023).
54. Pogostin, B. H., Linse, S. & Olsson, U. Fibril charge affects α-synuclein hydrogel rheological properties. *Langmuir* **35**, 16536–16544 (2019).
55. Biancalana, M. & Koide, S. Molecular mechanism of Thioflavin-T binding to amyloid fibrils. *Biochim. Biophys. Acta.* **1804**, 1405–1412 (2010).
56. Fusco, G. et al. Structural basis of membrane disruption and cellular toxicity by alpha-synuclein oligomers. *Science* **358**, 1440–1443 (2017).
57. Cascella, R. et al. The release of toxic oligomers from alpha-synuclein fibrils induces dysfunction in neuronal cells. *Nat. Commun.* **12**, 1814 (2021).
58. Holmes, B. B. et al. Heparan sulfate proteoglycans mediate internalization and propagation of specific proteopathic seeds. *Proc. Natl. Acad. Sci. USA* **110**, E3138–E3147 (2013).
59. Ihse, E. et al. Cellular internalization of alpha-synuclein aggregates by cell surface heparan sulfate depends on aggregate conformation and cell type. *Sci. Rep.* **7**, 9008 (2017).
60. Uversky, V. N., Lee, H. J., Li, J., Fink, A. L. & Lee, S. J. Stabilization of partially folded conformation during alpha-synuclein oligomerization in both purified and cytosolic preparations. *J. Biol. Chem.* **276**, 43495–43498 (2001).
61. Panuganti, V., Manchanda, K., Bharatam, P. V. & Roy, I. M14 substitutions in exanatide modulate alpha-synuclein aggregation. *FEBS J.* **293**, 1415–1432 (2026).
62. Miake, H., Mizusawa, H., Iwatsubo, T. & Hasegawa, M. Biochemical characterization of the core structure of alpha-synuclein filaments. *J. Biol. Chem.* **277**, 19213–19219 (2002).
63. Rozen, S. & Skaletsky, H. Primer3 on the WWW for general users and for biologist programmers. *Methods Mol. Biol.* **132**, 365–386 (2000).
64. McGlinchey, R. P. C-terminal alpha-synuclein truncations are linked to cysteine cathepsin activity in Parkinson's disease. *J. Biol. Chem.* **294**, 9973–9984 (2019).
65. Murray, I. V. Role of alpha-synuclein carboxy-terminus on fibril formation in vitro. *Biochemistry* **42**, 8530–8540 (2003).
66. Kardani, J., Sethi, R. & Roy, I. Nicotine slows down oligomerisation of α-synuclein and ameliorates cytotoxicity in a yeast model of Parkinson's disease. *Biochim. Biophys. Acta Mol. Basis Dis.* **1863**, 1454–1463 (2017).
67. Schreurs, S. et al. In vitro phosphorylation does not influence the aggregation kinetics of WT α-synuclein in contrast to its phosphorylation mutants. *Int. J. Mol. Sci.* **15**, 1040–1067 (2014).

68. Sot, B. et al. The chaperonin CCT inhibits assembly of α-synuclein amyloid fibrils by a specific, conformation-dependent interaction. *Sci. Rep.* **7**, 40859 (2017).
69. Nielsen, L. et al. Effect of environmental factors on the kinetics of insulin fibril formation: elucidation of the molecular mechanism. *Biochemistry* **40**, 6036–6046 (2001).
70. Thomas, P. & Smart, T. G. HEK293 cell line: a vehicle for the expression of recombinant proteins. *J. Pharmacol. Toxicol. Methods* **51**, 187–200 (2005).
71. Perfeito, R., Lazaro, D. F., Outeiro, T. F. & Rego, A. C. Linking alpha-synuclein phosphorylation to reactive oxygen species formation and mitochondrial dysfunction in SH-SY5Y cells. *Mol. Cell Neurosci.* **62**, 51–59 (2014).
72. Guo, C. et al. Inhibitory effects of magnolol and honokiol on human calcitonin aggregation. *Sci. Rep.* **5**, 13556 (2015).

Acknowledgements

The pRSETB-*α-SYN* construct was received as a kind gift from Prof. Roberto Cappai, University of Melbourne, Australia. Rabbit polyclonal α-SYN (1-10 amino acid) antibody was received as a gift from Prof. Masato Hasegawa, Department of Brain and Neuroscience, Tokyo Metropolitan Institute of Medical Sciences, Tokyo, Japan. We will like to thank Dr. Beena Krishnan (CSIR-IMTECH, Chandigarh) for providing us with the instrument facility to perform fluorescence polarization experiments. The confocal imaging facility of the National Agri-Food and Biomanufacturing Institute (BRIC-NABI, Mohali) is acknowledged. We would like to thank Abhiyanta Mukherjee and Sarath Chandra Devarakonda for help with microscopy imaging and protein purification, respectively. S.B. acknowledges the award of a senior research fellowship by ICMR (45/40/2022-DDI/BMS). Partial financial support from the Science and Engineering Research Board (CRG/2018/000458) is acknowledged.

Author contributions

S.B. carried out experiments and analyzed data, N.A.M. carried out rheology experiments and analyzed data, V.P. carried out cell-based studies and analyzed data, A.P. analyzed data and revised the manuscript, I.R. conceived and designed experiments, analyzed data and wrote the manuscript.

Competing interests

The authors declare no competing interests.

Additional information

Supplementary information The online version contains supplementary material available at https://doi.org/10.1038/s42004-026-02032-4.

Correspondence and requests for materials should be addressed to Ipsita Roy.

Peer review information Communications Chemistry thanks the anonymous reviewers for their contribution to the peer review of this work.